AMERICAN SOCIETY FOR MICROBIOLOGY | Molecular and Cellular Biology®

RESEARCH ARTICLE

# DHX33 Recruits Gadd45a To Cause DNA Demethylation and Regulates a Subset of Gene Transcription

**Weimin Feng,[a] Shiyun Chen,[a] Jiuling Wang,[a] Xingshun Wang,[a] Huaiyong Chen,[b,c] Wen Ning,[d] Yandong Zhang[a,e]***

[a]Department of Biology, Southern University of Science and Technology, Shenzhen, Guangdong, China
[b]Department of Basic Medicine, Haihe Clinic College of Tianjin Medical University, Tianjin, China
[c]Key Research Laboratory for Infectious Disease Prevention for State Administration of Traditional Chinese Medicine, Tianjin Institute of Respiratory Diseases, Tianjin Haihe Hospital, Tianjin, China
[d]School of Life Sciences, Nankai University, Tianjin, China
[e]Shenzhen KeYe Life Technologies, Co., Ltd., Shenzhen, China

**ABSTRACT** RNA helicase DHX33 was found to regulate the transcription of multiple genes involved in cancer development. But the underlying molecular mechanism remains unclear. Here, we found DHX33 associated extensively with gene promoters at CG-rich region. Its deficiency reduced the loading of active RNA polymerase II at gene promoters. Furthermore, we observed a functional interaction between DHX33, AP-2$\beta$, and DNA demethylation protein Gadd45a (growth arrest and DNA damage inductile protein 45a) at specific gene promoters. DHX33 is required to recruit GADD45a, thereby causing local DNA demethylation through further recruiting ten-eleven-translocation (Tet) methylcytosine dioxygenase enzyme, as manifested by reduced 5-hydroxymethyl cytosine levels for a subset of genes after DHX33 deficiency. This process might involve R-loop formation in GC skew as a guidance signal at promoter sites. Our report provides for the first time, to our knowledge, original evidence that DHX33 alters epigenetic marks and regulates specific gene transcription through interaction with Gadd45a.

**KEYWORDS** RNA helicase, DHX33, demethylation, CpG islands, Gadd45a, Aurora kinase

RNA helicase DHX33 belongs to the family of DEAD/DEAH box proteins, which have been found to play pivotal roles in every aspect of RNA metabolism (1). Although many RNA helicases are highly conserved from lower organisms to higher species, deregulation of these RNA helicases has been frequently observed in human diseases (2, 3). As one member of RNA helicase, DHX33 is found to be able to unwind RNA, DNA, or RNA/DNA duplexes with concomitant hydrolysis of ATP, thereby remodeling RNP or DNA/protein complexes (4). To date, we and other groups have identified DHX33 to be a multifunctional protein involved in various cellular activities. DHX33 protein has been found to regulate ribosome RNA transcription and mRNA translation as well as double-stranded RNA sensing during innate immunity activity (5–7). We further discovered that DHX33 associates with specific gene promoters to regulate mRNA transcription (8–10). Altered expression of DHX33 protein is frequently observed in various human cancers, including lung cancer, glioblastoma, breast cancer, lymphoma, and liver cancers (8–12). Despite all these efforts, the underlying molecular mechanism explaining how DHX33 regulates the transcription of these genes remains unclear.

Methylation of DNA cytosine acts as a major epigenetic modification to regulate gene expression and cellular activities (13). DNA methylation largely depends on DNA methyltransferases (DNMTs), which catalyze the transfer of a methyl group from S-ado-Met to cytosine (14). In mammals, DNA methylation primarily occurs in CG sites.

**Citation** Feng W, Chen S, Wang J, Wang X, Chen H, Ning W, Zhang Y. 2020. DHX33 recruits Gadd45a to cause DNA demethylation and regulates a subset of gene transcription. Mol Cell Biol 40:e00460-19. https://doi.org/10.1128/MCB.00460-19.



Address correspondence to Yandong Zhang, zhangyd@sustech.edu.cn.

* Present address: Yandong Zhang, Shenzhen KeYe Life Technologies Co., Ltd., Shenzhen, Guangdong, China.

**Received** 25 September 2019
**Returned for modification** 20 October 2019
**Accepted** 12 April 2020
**Accepted manuscript posted online** 20 April 2020
**Published** 15 June 2020

Normally, CpG-rich regions have a relatively lower methylation rate, which correlates with gene activation, while gene-specific methylation on CpG normally induces gene silencing (15). Active DNA demethylation is achieved by the 5-methylcytosin oxidation that is usually catalyzed by ten-eleven translocation (Tet) oxygenases, which convert 5-methylcytosine into 5-hydroxymethylcytosine, 5-formylcytosine, and 5-carboxylcytosine in sequential order (16). There are three different isoforms, Tet1 to Tet3, with differing tissue expression patterns and structural domains (17, 18). Tet1 is ubiquitous and plays important roles during embryo development (19). Active DNA demethylation frequently involves an important adaptor, the Gadd45 (growth arrest and DNA damage 45) family protein. There are three different isoforms, Gadd45a, Gadd45b, and Gadd45g (20, 21). Gadd45 normally promotes locus-specific DNA demethylation by recruiting Tet enzymes (22). How Gadd45 and Tet enzymes are recruited to a specific gene locus remains incompletely understood. Several mechanisms have been proposed. Epigenetic readers such as Ing1 have been found to read epigenetic marks to direct Gadd45a to H3K4me3 for DNA demethylation (23). Additionally, Gadd45a has been identified to be a RNA binding protein (24) that can be recruited by an R-loop (RNA-DNA hybrid) formed on a CG-rich region, which then guides the Tet enzyme for local DNA demethylation (25).

We previously discovered that a significant proportion of the cell transcriptome was altered due to DHX33 deficiency in cells. Despite our efforts, the underlying details of the molecular mechanism remain unknown. Here, we provide original evidence that RNA helicase DHX33 acts as an interacting partner for Gadd45a. DHX33, AP-2$\beta$, and Gadd45a form a functional complex on specific gene promoters. DHX33/AP-2$\beta$ complex is required for Gadd45a to be recruited into gene promoters, which then allows the recruitment of Tet1 enzyme for DNA demethylation. This process might be guided by R-loops in GC skew due to the function of DHX33. DHX33 knockdown caused the downregulation of 5-hydroxymethylcytosine associated with multiple genes in genome. Our report provides initial evidence for the function of DHX33 in regulating epigenetic signature through interaction with Gadd45a.

## RESULTS

**DHX33 deficiency reduces the loading of RNA Pol II on thousands of gene promoters.** We previously found that DHX33 actively participates in gene transcription. To delineate the changes in the cell transcriptome after DHX33 knockdown, we performed RNA polymerase II (Pol II) chromatin immunoprecipitation sequencing (ChIP-seq) analysis for cells that had been depleted for DHX33. H1299 cells were infected by lentivirus encoding either scrambled short hairpin RNA (shSCR) or shDHX33. After selection, equal numbers for cells were then subjected to chromatin immunoprecipitation with anti-phosphorylated polymerase II (anti-pPol II) (S2). DNA fragments were then sequenced. We discovered that the transcription of thousands of genes was influenced by DHX33 deficiency. Those highly affected genes fall into the categories of ribosome, cell cycle, RNA transport, ubiquitin mediated proteolysis, protein processing in endoplasmic reticulum (ER), mRNA surveillance, oocyte meiosis, and spliceosome, based on KEGG pathway analysis (Fig. 1A). DHX33 knockdown efficiency data are shown in Fig. 1B. Most notably, we found that the loading of RNA polymerase II on gene promoters was significantly abolished as shown in Fig. 1C. In control cells, activated RNA polymerase II bound to gene promoters, as shown by the distinct enrichment peak at the boundary between the upper 2 kb and the gene body. When DHX33 was knocked down in cells, the peak disappeared; this indicated that active RNA polymerase II failed to bind to the promoters. Additionally, we found that the binding efficiency for RNA polymerase II in DHX33 knockdown cells was significantly decreased compared to the control cell results. Furthermore, by comparing the peak Venn and gene Venn values (Fig. 1D), we discovered that transcription of over 3,000 genes was affected after DHX33 knockdown. We then compare the data to results of RNA-sequencing analysis of DHX33 knockdown cells. Of 560 genes that were identified to be downregulated by transcriptome sequencing (RNA-seq) in DHX33 knockdown cells, about 222 genes had

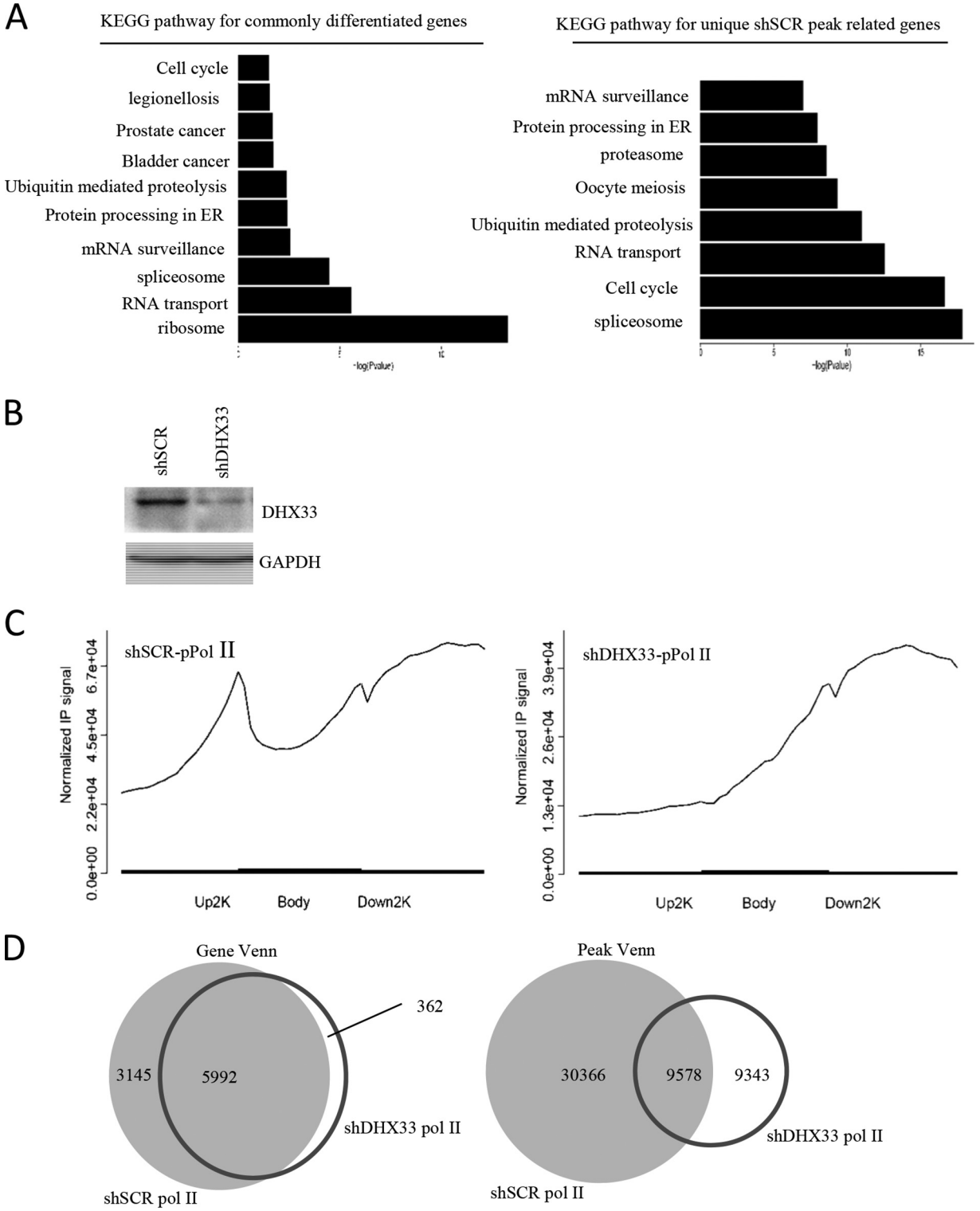


**FIG 1** DHX33 deficiency reduced the loading of RNA polymerase II on thousands of gene promoters. (A) Lung cancer cell line H1299 was infected with lentivirus encoding either shRNA-DHX33 or shSCR as a control. Five days postinfection, cells in equal numbers were subjected to chromatin immunoprecipitation analysis with anti-pPol II (S2); IgG was used as a control. Pooled DNA fragments were then sequenced and analyzed. Results of KEGG pathway analysis performed to identify genes differentiated between the two different samples are shown. (B) DHX33 knockdown analysis for shSCR and shDHX33 samples by Western blotting. GAPDH served as an internal control. (C) Normalized IP signal of RNA polymerase II on different gene domains (upstream 2 kb, gene body, and downstream 2 kb). The control is shown on the left, while the DHX33 knockdown sample is shown on the right. (D) Results of analyses comparing gene Venn values (left) and peak Venn values (right) between shSCR and shDHX33 samples.

loss of RNA Pol II occupancy on gene promoters (see File S3 in the supplemental material). In this gene list, we found Aurora kinase B (AURKB), E2F1, cyclin B, cyclin A, cyclin D, and MCM genes.

**DHX33 protein binds to gene promoters in the GC-rich region.** We previously discovered that DHX33 bound to gene promoters and regulated gene expression. To investigate how extensively DHX33 binds to genes across the genome and to determine its potential binding motif, we further performed chromatin immunoprecipitation followed by DNA sequencing with anti-DHX33 antibody. IgG was used as a negative control, and anti-pPol II (S2) was used as a positive control. As shown in the heat map of Fig. 2A, DHX33 bound extensively to the gene promoter region. On the basis of the enrichment signal, a distinct peak for DHX33 binding occurs in the junction between the upstream 2 kb and the gene body (Fig. 2B). This is consistent with the heat map data shown in Fig. 2A. We further discovered that the binding motif is most likely a CG-rich domain as shown by the motif analysis results (Fig. 2C). To check if DHX33 and active RNA Pol II cobound at transcriptional start sites (TSS), data sets from these two groups were compared. There were 328 genes with cobinding of DHX33 and pPol II at TSS. DHX33 preferentially bound to the GC-rich region in the upstream promoter, while pPol II bound to the proximal promoter; however, they might not overlap (see File S4 in the supplemental material). Over 10,000 peaks can be identified, and they are associated with nearly 8,000 genes. Results of KEGG pathway analysis of these captured genes are shown in Fig. 2D. Most genes fall into the categories of cell cycle, ubiquitin-mediated proteolysis, and cancer-related pathways, consistent with data in Fig. 1. To validate the results of ChIP-seq, we further conducted quantitative PCR (QPCR) analysis. Primers were designed to recognize the promoters of 9 representative genes, including *ART2*, *RPL11*, *PGK1*, *SIRT6*, *IP6K8*, *DOCK3*, *ART*, *BACH2*, and *RPS19*. As shown in Fig. 2E, DHX33 was highly enriched in the promoters of the genes mentioned above compared to the control. Data representing peak distributions for DHX33, IgG, and pPol II (S2) on representative chromosomes are shown in Fig. 2F.

**Transcription factor AP-2$\beta$ and DHX33 bind to the promoters of a subset of genes that partially overlap.** DHX33 has been found to bind to transcription factor AP-2$\beta$; the two form a functional complex in cells to regulate *Bcl-2* transcription (9). To examine how extensively this functional complex regulates other genes in cells, we performed ChIP-seq analysis for AP-2$\beta$, too. As shown in Fig. 3A, analysis of the AP-2$\beta$ binding sites on genes indicated that the proximal promoters of majority genes are the preferential binding sites for AP-2$\beta$ (Fig. 3A). Comparing the results to ChIP-seq data determined for DHX33, we found that there was a significant overlap of these two groups (Fig. 3B). Of 3,847 genes bound by AP-2$\beta$, 2,855 were also bound by DHX33 protein according to the results of peak-related gene analysis. Results of KEGG pathway analysis of the functions of these genes are shown in Fig. 3C. Gene ontology data for these two groups were partially consistent; for instance, genes involved in cell cycle processes (*MCM2*, *MCM4*, *CDC26*, *CCNB2*, *CCNE1*, *CCNE2*, and *CCND3*) were found in both AP-2$\beta$ and DHX33 groups. Our results indicate that AP-2$\beta$ and DHX33 may coregulate a subset of genes that play important roles in multiple aspects of cellular proliferation. To confirm this hypothesis, we further performed RNA-sequencing analysis for cells that had been knocked down for AP-2$\beta$. As shown in Fig. 3D, from the fragments per kilobase per million (FPKM) values, the indicated genes were consistently downregulated after AP-2$\beta$ knockdown. Those genes included *Bcl-2*, *AURK* genes, *MCM* genes, *cdc6*, *cyclin* genes, etc. Western blotting confirmed that AP-2$\beta$ was knocked down successfully in H1299 cells (Fig. 3E).

**DHX33 promotes gene transcription of Aurora kinase.** We previously found that expression of many important genes involved in cell proliferation, cell migration, and apoptosis was impaired due to DHX33 knockdown. Through RNA-sequencing analysis, we further discovered that DHX33 deficiency caused the downregulation of Aurora kinase family members. As shown in Fig. 4A, we found that both Aurora kinase A and Aurora kinase B were downregulated at the transcription level due to DHX33 deficiency

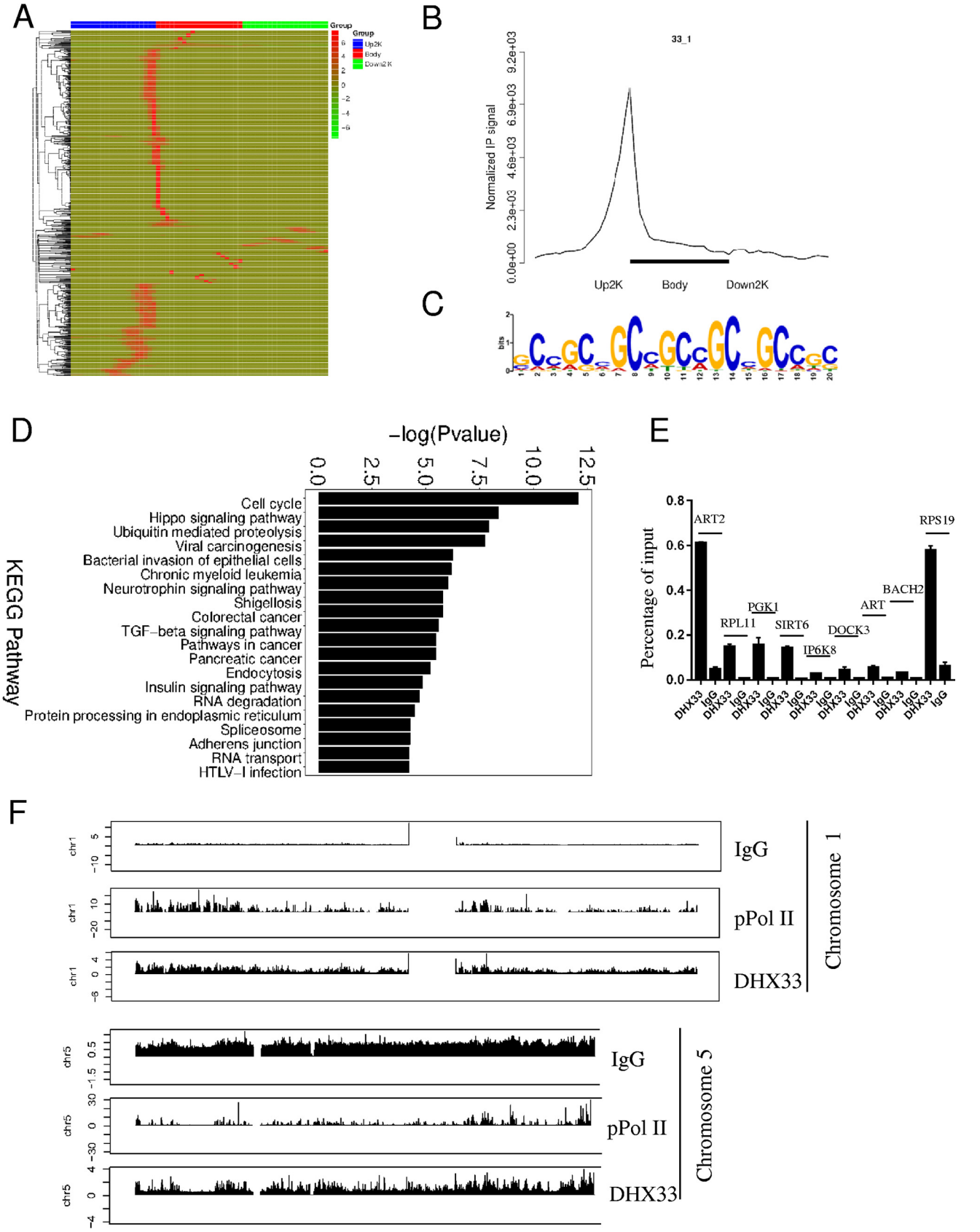


**FIG 2** DHX33 protein bound to the promoters of a subset of genes. (A) H1299 cells were infected by lentivirus encoding wild-type DHX33. Five days postinfection, cells were subjected to ChIP-seq analysis with anti-DHX33 antibody; IgG served as a negative control, and anti-pPol II served as a positive

(Continued on next page)

in H1299 and A549 lung cancer cell lines. We further performed QPCR analysis for Aurora kinase A/B in H1975 cells after DHX33 knockdown. We found the same result, as shown in Fig. 4B. To study whether the protein levels of Aurora kinase A and Aurora kinase B were decreased, we further performed Western blotting for DHX33-deficient cells. As shown in Fig. 4C and D, after DHX33 knockdown by short hairpin RNAs (shRNAs), the protein levels of both Aurora kinase A and Aurora kinase B were decreased dramatically. To confirm that the result that we obtained was not due to off-target effects of siRNA, we further performed DHX33 gene editing through the use of a CRISPR/Cas9 system. We constructed four different guide RNAs (gRNAs) targeting different DHX33 exons. Three of four gRNAs targeting DHX33 worked effectively to disrupt DHX33 expression after transient transfection of the plasmids into H1975 cells. The protein levels of both Aurora kinase A and Aurora kinase B were reduced significantly (Fig. 4E). To investigate whether the helicase activity of DHX33 is required to promote Aurora kinase A/B expression, we further performed protein overexpression analysis. As shown in Fig. 4F, we found that only the wild-type (WT) DHX33 was able to promote the expression of Aurora kinase B, while the helicase-defective mutant K94R DHX33 failed to do so. Next, to investigate whether DHX33 alone or the DHX33/AP-2$\beta$ complex regulates Aurora kinase expression, we analyzed the expression of Aurora kinases after AP-2$\beta$ knockdown (Fig. 4G and H). The levels of both protein and mRNA of Aurora kinase B and A were decreased. In Ras-initiated lung tumorigenesis, we found that DHX33 was induced after Ras activation. In this situation, we found that both Aurora kinase A protein and Aurora kinase B protein were upregulated as shown by the immunohistochemistry staining (Fig. 4I). However, when we genetically deleted DHX33 gene in lung epithelial cells, expression of both Aurora A and Aurora B was decreased at the protein level (Fig. 4J). Our results demonstrate that DHX33 was able to regulate expression of Aurora kinase A and B expression both in cells and in mouse models.

**DHX33 binds to the promoter of the Aurora kinase B gene.** To dissect the molecular mechanism of gene regulation by DHX33, we chose the Aurora kinase B gene as a representative gene for further study. We first performed chromatin immunoprecipitation analysis with a set of primers scanning the genomic region surrounding the transcription start site of the Aurora kinase B gene to determine the potential binding sites of DHX33 in the Aurora kinase B gene. As shown in Fig. 5A, we designed multiple pairs of primers within 4 kb both upstream and downstream of the transcriptional start sites. Sequence information for the primers is shown in Table 1. The results of the ChIP analysis are shown in Fig. 5B. DHX33 appears to preferentially bind to a proximal site upstream of the start site. To study whether the helicase-defective DHX33 mutant would be able to bind to the gene promoter, we performed ChIP analysis for both the wild-type (WT) strain and helicase-defective DHX33 mutant (K94R). As shown in Fig. 5C, both proteins bound to the gene promoter. The DHX33 overexpression level in H1299 cells can be seen in Fig. 5D.

**DHX33, Gadd45a, and AP-2$\beta$ form a complex on gene promoters.** We frequently observed DHX33 bound to gene promoters and thereby regulated gene expression. However, how DHX33 is able to regulate so many different genes at the transcription level remains unknown. In eukaryotic cells, DNA methylation plays an important role in gene regulation. Gadd45a is an important adaptor protein which recruits Tet enzyme to cause DNA demethylation. Here, we found that Gadd45a is a binding partner of DHX33. We performed protein coimmunoprecipitation analysis for DHX33 in H1299

**FIG 2** Legend (Continued)
control. The heat map shows the binding region (red) of DHX33 on different gene domains. The scale bar is shown on the right. (B) Normalized IP signal analysis for DHX33 on gene regions. (C) Motif analysis for DHX33 binding sites on genes. The most preferential motif is shown to be a CG-rich region. (D) KEGG pathway analysis of genes associated with DHX33 protein. Most fall into the categories of cell cycle, ubiquitin-mediated proteolysis, and cancer-related pathways. TGF-beta, transforming growth factor beta; HTLV-1, human T-cell leukemia virus type 1. (E) To validate the results for ChIP sequencing, quantitative PCR was conducted for pooled DNA fragments from the ChIP analysis performed as described for panel A. Nine representative genes were selected from the gene list. Enrichment signals are plotted as the input percentage. All demonstrated significant difference compared to the IgG control. (F) Peak distribution analysis for ChIP signals from IgG, anti-pPol II, and anti-DHX33 antibody. Results from two representative chromosomes are shown. The data for the whole genome can be found in the supplemental material. *y*-axis data represent the fold enrichment values.

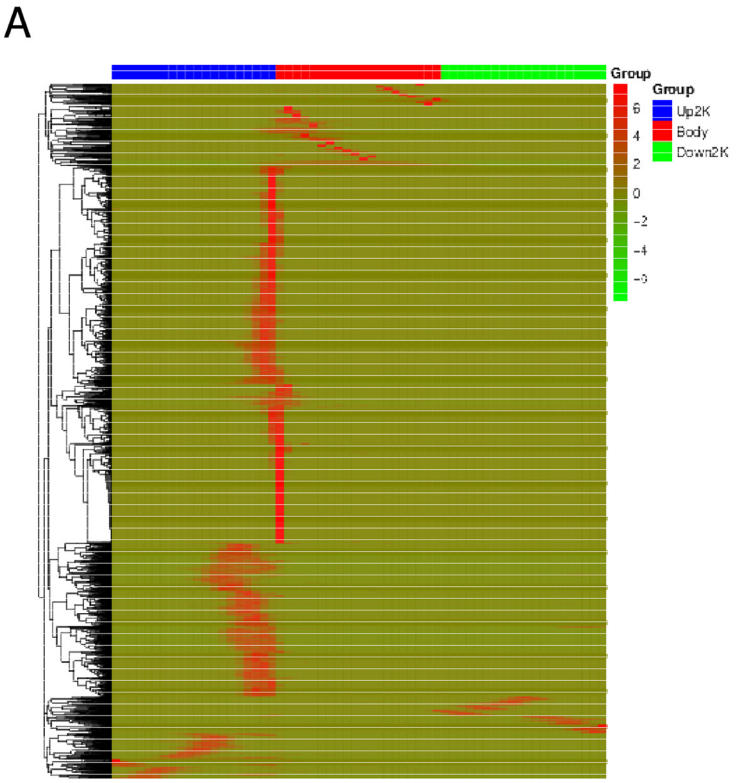


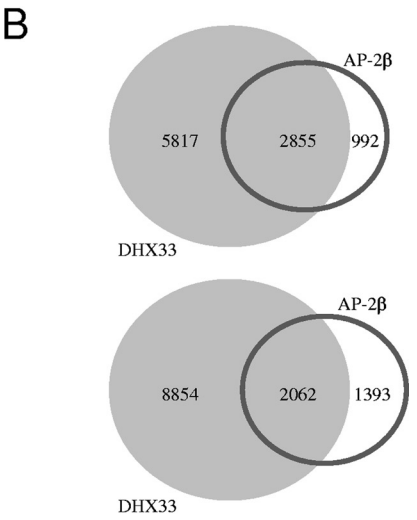


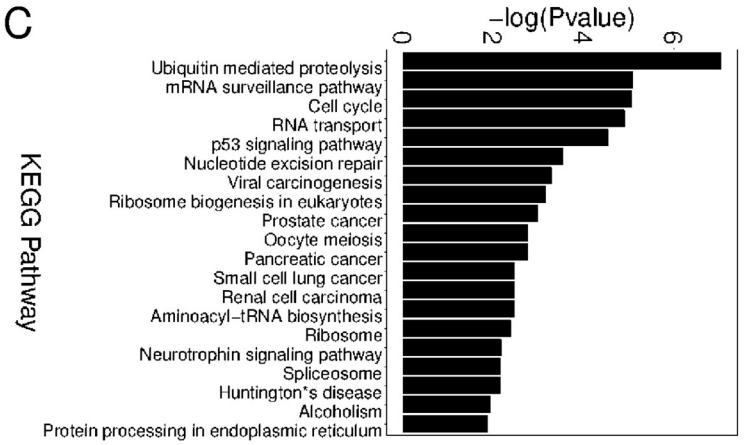


D

| gene name | shSCR | shAP-2β |
|---|---|---|
| TFAP2B | 0.01 | 0 |
| BCL-2 | 0.99 | 0.76 |
| AURKA | 118 | 107 |
| AURKB | 114 | 70 |
| AURKC | 0.05 | 0.07 |
| MCM2 | 66 | 33 |
| MCM3 | 67 | 44 |
| MCM4 | 78 | 46 |
| MCM5 | 65 | 35 |
| MCM6 | 48 | 31 |
| MCM7 | 334 | 191 |
| MCM8 | 16.6 | 11.6 |
| MMP9 | 0.73 | 0.09 |
| MMP14 | 33 | 23 |
| FEN1 | 24 | 11 |
| CCNA1 | 8.2 | 2.4 |
| CCNB1 | 168 | 141 |
| CCNB2 | 130 | 117 |
| CCND1 | 79 | 71 |
| CCND2 | 1.46 | 0.85 |
| CCNL2 | 119 | 61 |
| PCNA | 137 | 84 |

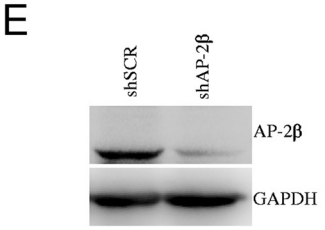


**FIG 3** Transcription factor AP-2$\beta$ and DHX33 bound to the promoters of a subset of genes that partially overlapped. (A) H1299 cells were subjected to ChIP-seq analysis with anti-AP-2$\beta$ antibody; IgG was used as a control. Over 3,000 genes were found to associate with AP-2$\beta$. The heat map shows the binding region (red) of AP-2$\beta$ on different gene domains. The scale bar is shown on the right. (B) Data representing the population were compared to ChIP-seq data from anti-DHX33. Gene Venn values (top) and peak Venn values (bottom) are shown. Over 2,800 genes were found to be bound by both DHX33 and AP-2$\beta$ proteins. (C) KEGG pathway analysis of genes associated with AP-2$\beta$ protein. (D) RNA sequencing was performed for RNA samples extracted from H1299 cells after AP-2$\beta$ was knocked down. The FPKM values determined for a subset of genes involved in cell cycle or apoptosis are shown. (E) Western blotting was performed to confirm that AP-2$\beta$ was efficiently knocked down in H1299 cells. GAPDH served as an internal control.

A

| cell line | gene name | shSCR | shDHX33 |
|---|---|---|---|
| H1299 | DHX33 | 10.5 | 2.76 |
| | Aurora kinase A | 92.75 | 14.57 |
| | Aurora kinase B | 55.19 | 12.3 |
| | Aurora Kinase C | 0.207 | 0.524 |
| A549 | DHX33 | 16.3 | 3.2 |
| | Aurora kinase A | 66.6 | 19.1 |
| | Aurora kinase B | 56.98 | 11.5 |
| | Aurora kinase C | 0.24 | 0.24 |

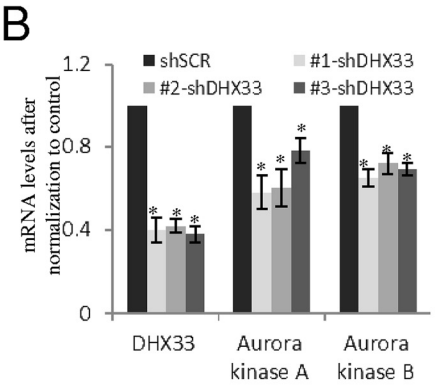


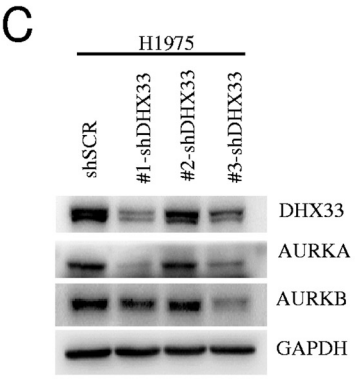


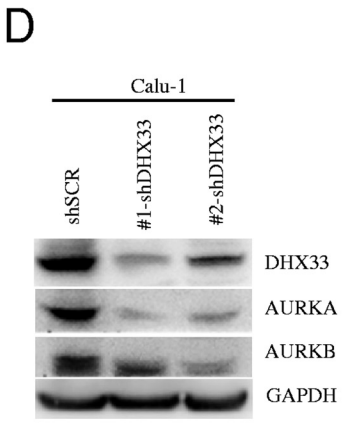


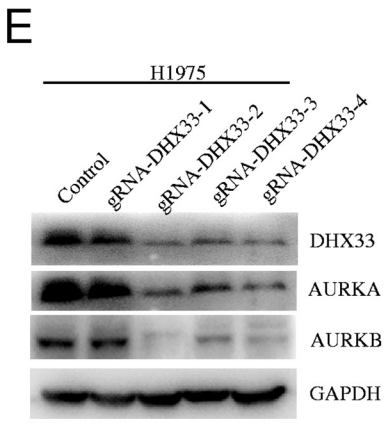


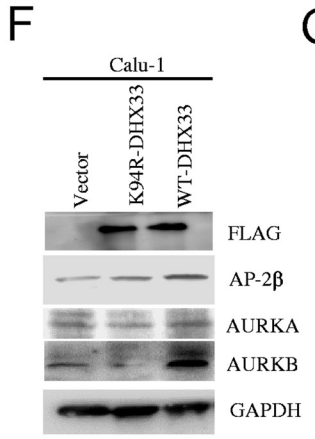


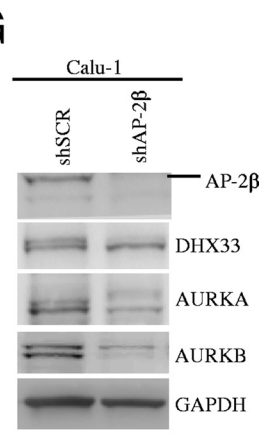


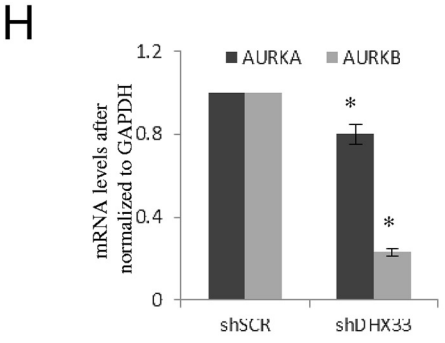


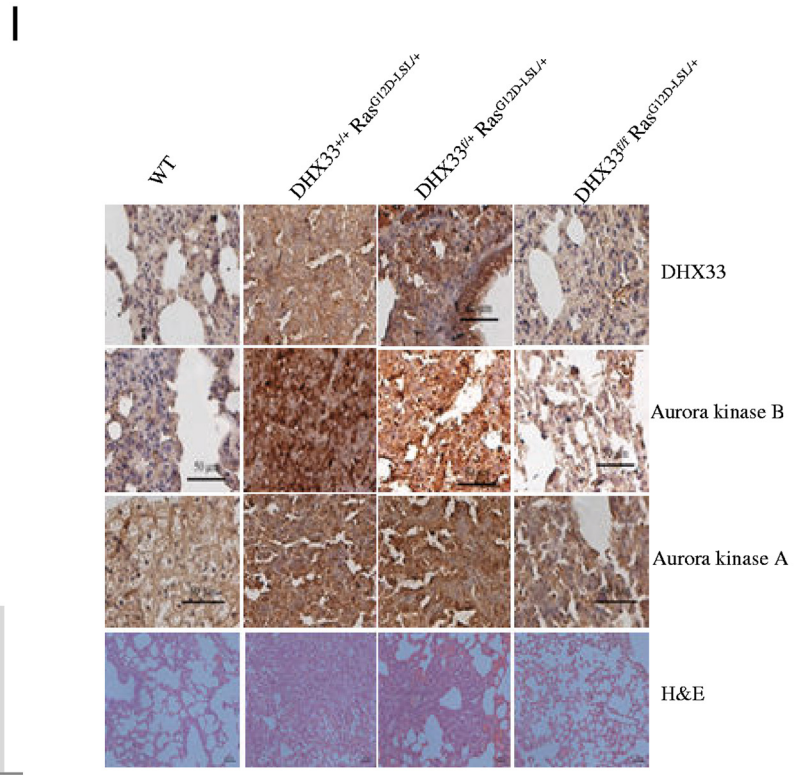


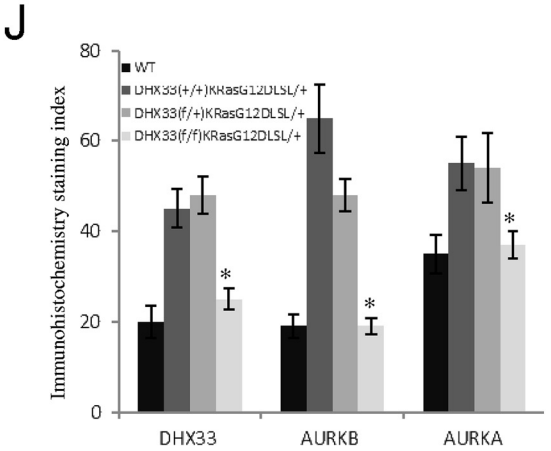


**FIG 4** DHX33 promoted gene transcription of Aurora kinase A/B. (A) RNA-seq was performed on H1299 or A549 cells after DHX33 was knocked down. The expression levels of Aurora kinase are shown. Both Aurora kinase A and Aurora kinase B were downregulated, while Aurora kinase C was either not affected

(Continued on next page)

cells. As shown in Fig. 6A, with or without RNase H1, DHX33 formed a complex with Gadd45a but not with Tet1 enzyme in our experimental setting. This indicates that the formation of this complex is not dependent on RNA. To examine whether AP-2$\beta$ participates in this complex, we further performed immunoprecipitation analysis for AP-2$\beta$. We found that AP-2$\beta$ interacted with both Gadd45a and DHX33; this interaction was not dependent on RNA either (Fig. 6B). To confirm these interactions, we further performed reciprocal immunoprecipitation as described for Fig. 6C and D. Our results indicate that these three proteins probably associated with each other to form a ternary complex. The interaction between them was insensitive to RNase H1 treatment. To confirm the interaction between them, we further performed immunofluorescence analysis. As shown in Fig. 6E, we performed pairwise colocalization study for these three proteins. They partially colocalized in cell nuclei but not in the cytosol. To study whether the helicase activity of DHX33 is involved in the binding between DHX33 and Gadd45a as well as AP-2$\beta$, we further compared the binding efficiencies of these proteins to the results seen with the wild type and the helicase-defective DHX33. As shown in Fig. 6F, the K94R DHX33 mutant was still able to interact with AP-2$\beta$; however, the binding of Gadd45a to DHX33 was reduced as a consequence of the loss of DHX33 helicase activity. Finally, to investigate whether these proteins interact with each other at the Aurora kinase gene promoter, we performed re-ChIP analysis with anti-Gadd45a and anti-DHX33 (Fig. 6G), as well as re-ChIP analysis with anti-DHX33 and anti-AP-2$\beta$ (Fig. 6H). We found that DHX33, AP-2$\beta$, and Gadd45a formed a complex on the same promoter. We further performed chromatin immunoprecipitation analysis with the DHX33 K94R protein. As shown in Fig. 6I, the mutant was much less efficient at assembling DNA demethylation protein Gadd45a on the Aurora kinase B gene promoter.

**DHX33 is important to recruit DNA demethylation proteins to gene promoters.** Gadd45a protein functions as an important adaptor in DNA demethylation. To investigate whether the DHX33/AP-2$\beta$/Gadd45a complex is functional, we further analyzed the recruitment of DNA demethylation proteins on gene promoters with or without DHX33/AP-2$\beta$. We performed gene knockdown by shRNA-DHX33 or shRNA-AP-2$\beta$ as before. As shown in Fig. 7A and B, DHX33 or AP-2$\beta$ deficiency markedly decreased the loading of Gadd45a and Tet1 on the Aurora kinase B promoter. We further analyzed the product of the first step during active DNA demethylation, 5-hmC, on the Aurora B gene. As shown in Fig. 7C, after DHX33 knockdown, the level of 5hmC on the Aurora kinase B gene was decreased significantly. DNA demethylation usually correlates with histone acetylation (26). We further analyzed the levels of histone H4 acetylation with or without DHX33/AP-2$\beta$. As shown in Fig. 7D, DHX33 or AP-2$\beta$ knockdown dramatically reduced the levels of H4 acetylation. The knockdown efficiency was analyzed by Western blotting as shown in Fig. 7E. DHX33 or AP-2$\beta$ knockdown could not influence the expression of Gadd45a or Tet1 protein. We further mapped the details of the DNA methylation sites by sodium bisulfite treatment followed by DNA sequencing (Fig. 7F). Due to DHX33 deficiency, the methylation rate increased by ~70% in a CG island upstream of the gene transcription start site (9 of 13 CGs were methylated), while the

**FIG 4** Legend (Continued)
or slightly upregulated. (B) The mRNA levels of Aurora kinase A and B were analyzed by QPCR after DHX33 knockdown in H1975 cells. GAPDH was used for normalization. *, $P < 0.05$; $n = 3$. (C and D) H1975 (C) and Calu-1 (D) cells were infected by lentivirus encoding either shSCR or multiple shDHX33s. Four days postinfection, whole-cell extracts were prepared and subjected to Western blotting with the indicated antibodies. GAPDH was used as an internal control. (E) H1975 cells were transfected by plasmids encoding Cas9 and guide RNAs targeting different exons of DHX33 gene, with empty vector as a control. Two days posttransfection, whole-cell extracts were subjected to Western blotting with the indicated antibodies. GAPDH served as an internal control. (F) Calu-1 cells were infected with lentivirus encoding empty vector, the K94R helicase-defective DHX33 mutant, or wild-type DHX33. Four days postinfection, whole-cell extracts were subjected to Western blotting with the designated antibodies. (G) Calu-1 cells were infected with lentivirus encoding either shSCR or shAP-2$\beta$. Four days postinfection, whole-cell extracts were subjected to Western blotting with the designated antibodies. (H) Total RNA was extracted from Calu-1 cells in 4G and then subjected to reverse transcription-PCR (RT-PCR) analysis for the expression of Aurora kinase A and B. *, $P < 0.05$; $n = 3$. (I) Mice with the four different genotypes were treated with adenovirus encoding Cre recombinase according to a standard protocol (28). Lung tissues from the four designated groups were analyzed 2 months later; immunohistochemistry staining was performed with the indicated antibody for gene expression analysis. Tissues were then counterstained with hematoxylin (blue). Brownish coloring indicates positive staining. Hematoxylin and eosin (H&E) staining results are also shown at the bottom. (J) Quantitation of the immunohistochemistry (IHC) signals. Five representative areas were selected for evaluation of IHC signals. *, $P < 0.05$; $n = 5$.

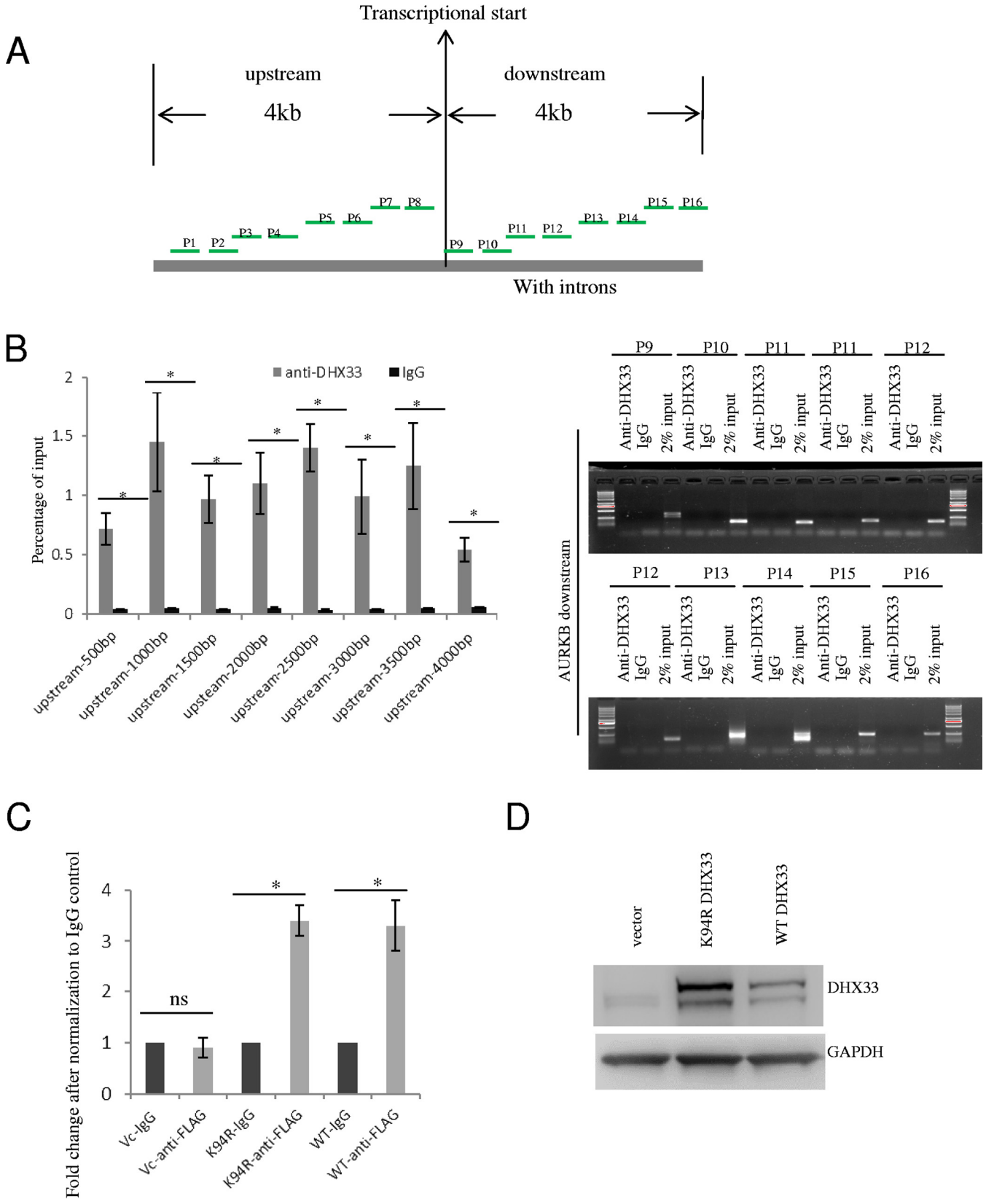


**FIG 5** DHX33 bound to the proximal promoter region of Aurora kinase B gene. (A) Diagram showing the positions of different primer sets for analyzing the binding position of DHX33 on the Aurora kinase B gene. A range of upstream 4 kb to downstream 4 kb of the gene body is chosen. (B) Results of ChIP analysis using the different pairs of primers. H1299 cells were subjected to ChIP analysis with anti-DHX33 antibody; IgG was used as a control. For the upstream gene promoter region, DNA samples were used as described for the quantitative PCR analysis. The data are presented as percentages of input. *, $P < 0.05$; $n = 3$.

(Continued on next page)

**TABLE 1** Primer sequences used in ChIP analysis for searching the DHX33 binding sites on the Aurora kinase B promoter

| Primer name | Primer direction | AURKB primer sequence (5′ to 3′) |
|---|---|---|
| P1 | Forward | CTAGATCATACCCTCTTCGTCCA |
| | Reverse | TCCACGGGTTCAGCTCTCA |
| P2 | Forward | GCCAACGTAATGAAACCCCGTC |
| | Reverse | AATCTCGGCTCACTGCAACCTC |
| P3 | Forward | GCCAACGTAATGAAACCCCGTC |
| | Reverse | AATCTCGGCTCACTGCAACCTC |
| P4 | Forward | TCCGCCTCCCAGGTTCAAGC |
| | Reverse | CCAACACAGTGAAACCCGTCT |
| P5 | Forward | CTCAAGTGATACAGCCGCCTT |
| | Reverse | TGAGCCTCTACATGCCTACGTT |
| P6 | Forward | GCTCACGCCTGTAATCCAAGCA |
| | Reverse | CTGTCTCAGCCTCCCGAGT |
| P7 | Forward | TAATTGGGGCTCATTTCTGGACCT |
| | Reverse | ACGGGGTTTCATCACATTGCTC |
| P8 | Forward | ACTACAGAAACCGACTGCAT |
| | Reverse | TGGGCCTTCTATGAAATAACCAGTG |
| P9 | Forward | CTCATTCCGCCTCTTCCATTGGGTT |
| | Reverse | GCCAGCCCAACGGACCCTCT |
| P10 | Forward | GTTTGACGACAGAACCCGCTCT |
| | Reverse | CCCTGCCTGCTCAGTCCCA |
| P11 | Forward | CCTCTCTGATTTGAAATGCCAC |
| | Reverse | CCCTAGGCCCCAAATAGTGA |
| P12 | Forward | CCTTAAAGCCTGTTCTTGCAAA |
| | Reverse | GAGCTGCGTCAATGAACACC |
| P13 | Forward | TGTGAGTCCTTTGCCCCTT |
| | Reverse | CGCCTGTAATCCCAGCTACTCG |
| P14 | Forward | CTGACCTTGTGATCCGCCTG |
| | Reverse | CCCCAATTCAAAGAGAAACACTGA |
| P15 | Forward | ATCTTAACGTAAGTGCCCCAAGCC |
| | Reverse | TCATCAATTGTGAAGTGCCGCCTG |
| P16 | Forward | CCTCCAGTTTCCCCTTACCAC |
| | Reverse | GCTCTTCTGCAGCTCCTTGT |

control sample demonstrated no methylated CGs at all. ChIP-PCR analysis was further performed, and the results showed that DHX33 knockdown led to disengagement of AP-2$\beta$ on the Aurora kinase B promoter (Fig. 7G). As expected, this caused the loading of active RNA polymerase II onto the promoter to be markedly reduced (Fig. 7H). The DHX33 knockdown efficiency data are shown in Fig. 7I. To confirm that the Gadd45a/Tet1 pathway mediated gene regulation by DHX33, we further interrupted Gadd45a

**FIG 5** Legend (Continued)
For the downstream 4-kb region of the gene body, data are presented as gel images after PCR amplification; 2% input was used as a control. (C) H1975 or H1299 cells were infected by lentivirus encoding empty vector, K94R mutant of DHX33, or wild-type DHX33. Five days postinfection, cells in equal numbers were subjected to ChIP analysis with anti-FLAG antibody; IgG was used as a control. Primer set 8 was used for PCR amplification. Quantitative PCR was performed, and data are presented as fold enrichment in comparison to the IgG control. *, $P < 0.05$; $n = 3$. (D) Western blotting of whole-cell extracts (H1299) with the indicated antibodies.

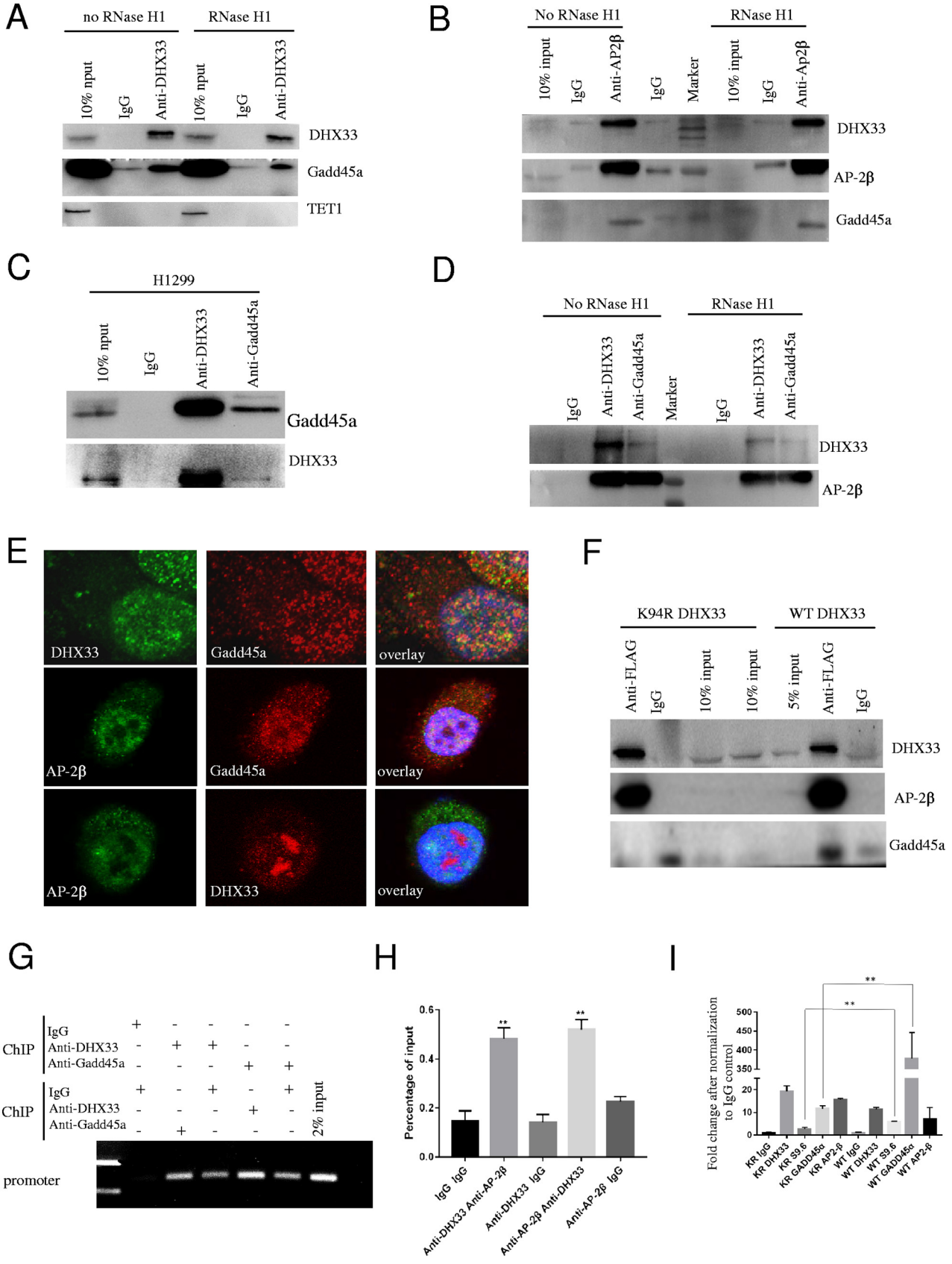


**FIG 6** DHX33, Gadd45a, and AP-2$\beta$ formed a complex on the Aurora kinase B gene promoter region. (A) Whole-cell extract of H1975 cells was treated either with RNase H1 or without RNase H1. The total cell lysates were immunoprecipitated with anti-DHX33 antibody; IgG was used as a control. Western blotting

(Continued on next page)

and Tet1 by the use of shRNAs. As shown in Fig. 7J, in both situations, the transcription of Aurora kinase B was downregulated by knockdown of either Gadd45a or Tet1.

Previous studies had shown that Gadd45a recognized the R-loop structure in a GC-rich region to guide the Tet enzyme for DNA demethylation; therefore, we performed ChIP analysis with the specifically R-loop-recognizing antibody, S9.6. As shown in Fig. 7K, formation/stability of the R-loop was abolished in the promoter of Aurora kinase B due to DHX33 silencing. Our data support the theory that the R-loop may guide Gadd45a to gene promoters in a DHX33-dependent manner.

**DHX33 alters epigenetic marks for a subset of genes.** Reduced DNA demethylation might at least partially explain gene deactivation in Aurora kinase B after DHX33 knockdown. But whether or not this would apply to other downstream genes of DHX33 remains an issue. To analyze the global effect of DHX33 on epigenetic marks, we further performed 5hmC-DNA immunoprecipitation (5hmC-DIP) analysis for H1299 cells after DHX33 knockdown. The results are shown in Fig. 8A. Changes of 5-hmC levels were observed for many genes. On the basis of gene Venn and peak Venn analysis, over 3,000 unique peak-related genes were found to have alterations for their 5-hmC marks; both DNA demethylation and DNA methylation occurred due to DHX33 deficiency. Data representing distributions of peaks and fold enrichment of 5-hmC are shown in Fig. 8B. Predominantly, 5-hmC accumulated in the upstream 2-kb region and gene body and we could not detect a significant difference between the control and DHX33 knockdown group in the 5-hmC levels at the genomic level. Results of KEGG pathway analysis performed to identify differential levels of gene expression (>2-fold difference) are shown in Fig. 8C (top). Among the genes examined, many of those involved in cancer pathways were found to be affected due to DHX33 deficiency. Functions for the unique shSCR peak-related genes are listed in Fig. 8C (bottom), and many of those are involved in cellular signaling pathways of cancer. The function of DHX33 with respect to 5-hmC levels for specific genes can be shown by taking Bcl-2 gene as an example. We found that the 5-hmC level determined for the Bcl-2 gene (primarily in the gene body) was markedly reduced after DHX33 knockdown (Fig. 8D).

We further analyzed methylation with respect to the whole genome (capturing known methylation sites with a SeqCap Epi enrichment system). As shown in Fig. 9A, comparing shSCR control and DHX33 knockdown samples, we found the DHX33 deficiency led to an overall increase in the number of methylation sites at the genomic level from 4,405,642 to 5,678,794 sites in total. Notably, the methylation pattern of C changed, too. In mammalian cells, 5mC predominantly occurs on CG. However, when DHX33 was knocked down, the percentages of two other methylcytosine forms, mCHG and mCHH, increased dramatically, from 0.45% (in control samples) to 10.39% and 5.36% (in DHX33 knockdown samples), respectively. The functional relevance of these results remains to be revealed.

Among 185,997 differential 5-methylcytosine/5-hydroxylmethylcytosine sites that were found to be relevant to genes, KEGG pathway analysis indicated that many of the genes belong to pathways in cancer (Fig. 9B), for instance, Bcl-2, Aurora kinase A, and

**FIG 6** Legend (Continued)
was performed in order to analyze the interaction of Gadd45a and Tet1 with DHX33 on the immunocomplexes. (B) Total cell lysates with or without RNase H1 treatment were immunoprecipitated with anti-AP-2$\beta$ antibody; IgG was used as a control. Western blotting was performed to detect the interaction of DHX33 and Gadd45a with AP-2$\beta$. (C) Whole-cell extracts from H1299 cells were reciprocally immunoprecipitated with either anti-DHX33 or anti-Gadd45a, with IgG as a control. Western blotting was performed with the indicated antibodies. (D) Total cell lysates of H1299 cells with or without RNase H1 treatment were immunoprecipitated with anti-DHX33 or anti-Gadd45a antibody, with IgG as a negative control. Western blotting was performed with the indicated antibodies to confirm the interaction between them. (E) H1299 cells were fixed for immunostaining with three different pairs of antibodies. DAPI demarked cell nuclei. Partial colocalization was observed between DHX33 and Gadd45a, AP-2$\beta$ and DHX33, and AP-2$\beta$ and Gadd45a in the cell nuclei. (F) H1299 cells were infected with either FLAG-tagged wild-type DHX33 (WT DHX33) or K94R mutant DHX33. Cells were then subjected to immunoprecipitation analysis with anti-FLAG antibody; IgG was used as an internal control. Western blotting was performed to detect the interaction of DHX33 with Gadd45a and AP-2$\beta$. (G) H1299 cells were subjected to re-ChIP analysis. The first IP experiment was performed either with anti-DHX33 antibody or with anti-Gadd45a antibody, while the second IP was performed with the other antibody. Compared to controls, DHX33 and Gadd45a were found to bind to the same promoter region of Aurora kinase B. (H) A similar experiment was performed to detect the interaction of DHX33 and AP-2$\beta$ on the Aurora kinase B gene promoter. Data represent the percentage of input for each sample, *, $P < 0.05$; $n = 3$. (I) H1299 cells were infected with either FLAG-tagged wild-type DHX33 (WT DHX33) or K94R (KR) mutant DHX33. Equal numbers of cells were then subjected to chromatin immunoprecipitation analysis with the indicated antibody. The occupancy of DHX33, AP-2z$\beta$, and Gadd45a on an AURKB gene promoter was analyzed by QPCR. Data were plotted as fold changes against IgG control. **, $P < 0.02$, $n = 3$.

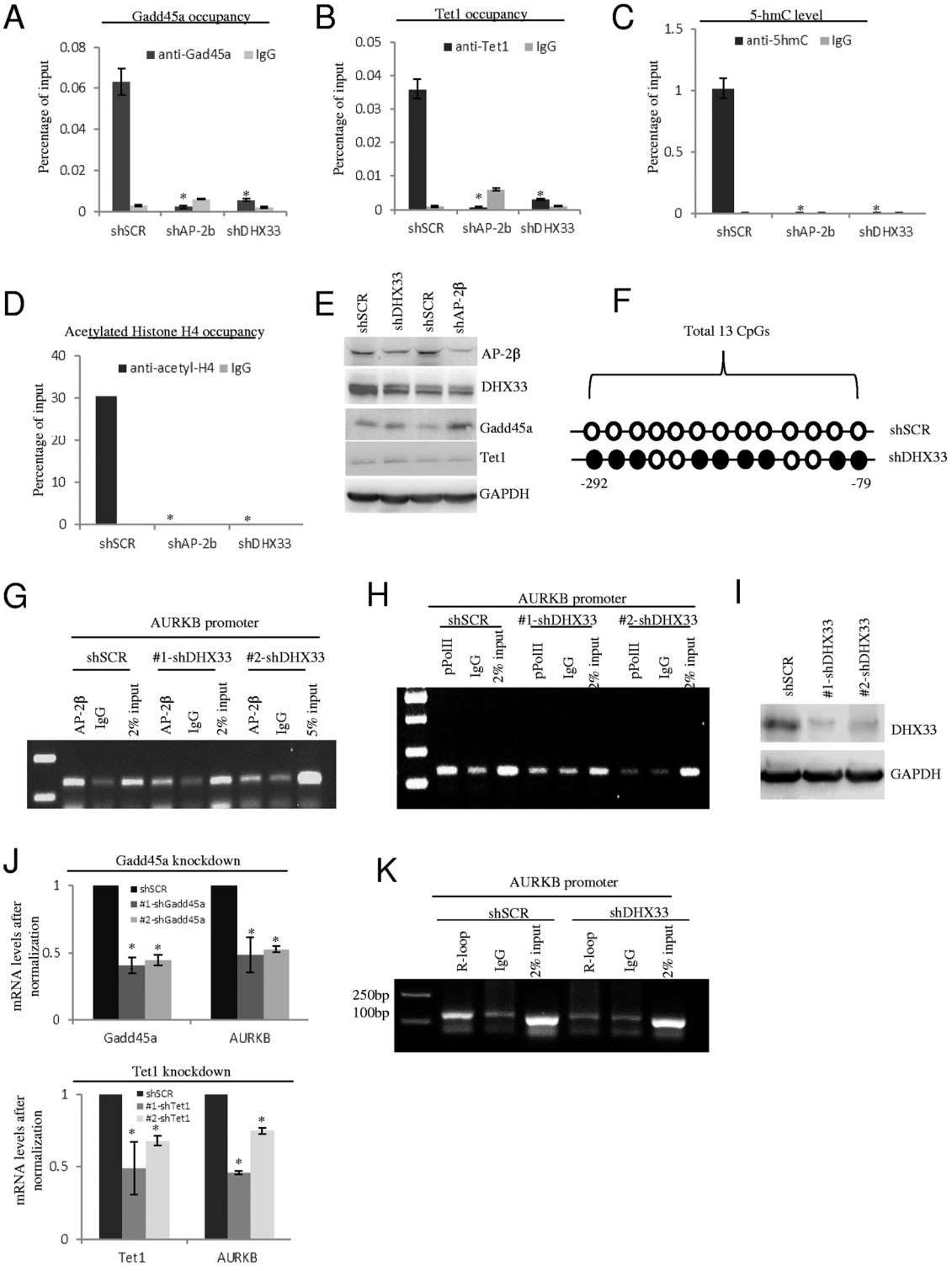


**FIG 7** DHX33 is important to recruit DNA demethylation proteins to gene promoters. (A to D) H1299 cells were infected by lentivirus encoding shSCR, shAP-2$\beta$, or shDHX33. Five days postinfection, cells in equal numbers were subjected to ChIP analysis with anti-Gadd45a antibody (A), anti-Tet1 (B), anti-5-hmC (C), or anti-acetyl-H4 (D); IgG was used as a control. Quantitative PCR was performed to evaluate the enrichment signals. *, $P < 0.05$; $n = 3$. (E) Western blotting was performed to check the knockdown efficiency of DHX33 or AP-2$\beta$, as well as the protein levels of Gadd45a and Tet1, with shSCR as a control. (F) Genomic DNA samples were prepared from DHX33 knockdown cells and were further subjected to DNA methylation analysis with an EZ DNA methylation gold kit. Of 13 CGs in a CG island, 9 were methylated, as shown by the closed circles. Open circles indicate nonmethylated CG. (G to I) Five days after infection by lentivirus, the H1299 cells mentioned above (shSCR, shRNA-DHX33) were fixed by the use of 1% formaldehyde and were then subjected to ChIP analysis with anti-AP-2$\beta$ (G) or anti-pPol II (phosphorylation on S2 of the C-terminal domain [CTD]) (H), with IgG as a control. Samples were then analyzed by PCR and PAGE gel analysis. DHX33 knockdown efficiency data

(Continued on next page)

PLAU genes. Notably, a significant portion of the differentially expressed genes are involved in synaptic signaling. The methylation levels are also presented in a violin graph (Fig. 9C). For the differentiated DNA methylation sites, a significant increase was observed on CG islands (Fig. 9D). The levels of 5-mC and 5-hmC were upregulated or downregulated by DHX33, again revealing the complicated roles of DHX33 in epigenetic regulation.

## DISCUSSION

In previous studies, we had observed that DHX33 regulated specific gene transcription through associating with promoters. In this study, we carried the DHX33 study to the genomic level and found that DHX33 regulated thousands of genes, indicating the pivotal role of DHX33 in modulating the cellular transcriptome. At the current stage of investigation, we were unable to conclude that all these genes would be directly regulated by DHX33. In the present study, we focused on the subset of genes that were positively regulated by DHX33 directly. Among these genes, we found that DHX33 regulated the epigenetic marks through recruiting DNA demethylation proteins. This process might be guided by an R-loop on the CG islands on gene promoters (as shown in the Fig. 10 diagram), in a DHX33-dependent manner. DHX33 deficiency leads to disengagement of active RNA polymerase II at gene promoters, but the disengagement occurs toward the gene body or the 3′ end of genes. This might be interpreted as the transcriptional complex elongating faster or accumulating at the end of genes due to a defect in transcriptional termination. However, as the transcription rates were decreased for this subset of genes, this could not be a result of accelerated elongation. Additionally, the IP signals for RNA polymerase II in DHX33-deficient cells were generally lower than those seen with the control ($3.9 \times 10^4$ versus $6.7 \times 10^4$). This could not be a result of defect in transcriptional termination.

Transcription factor AP-2$\beta$ was previously identified as a binding partner of DHX33. The two proteins were found to work together to regulate Bcl-2 gene transcription. In this study, genome-wide ChIP-seq analysis was conducted for both AP-2$\beta$ and DHX33. The genes that are bound by AP-2$\beta$ and DHX33 overlap significantly. Other than the Bcl-2 gene, over 2,000 genes can be bound by both DHX33 and AP-2$\beta$ at the promoter region. These genes play important roles in cell cycle and cancer development. Additionally, we identified a novel protein interaction partner on the DHX33/AP-2$\beta$ complex, Gadd45a. Gadd45a is known for its pivotal function in active and locus-specific DNA demethylation. DHX33, Gadd45a, and AP-2$\beta$ form a functional complex to regulate gene expression through altering epigenetic marks.

We found that the levels of the first product seen during active DNA demethylation, 5-hmC, decreased significantly at specific gene loci after DHX33 or AP-2$\beta$ knockdown. Elevated 5-hmC levels on a gene body normally indicate gene transcriptional activation. DHX33 deficiency caused the reduction of 5-hmC levels on the promoter of Aurora kinase B, with concomitant elevation of DNA methylation on CGs. Furthermore, DHX33 was initially identified as an important player in regulating ribosome RNA biogenesis. In the current study, we found that DHX33 and Gadd45a colocalized significantly in the nucleoli. Gadd45a has been found to positively regulate ribosome DNA transcription through DNA demethylation via nucleotide excision repair (NER). It is possible that DHX33 and Gadd45a work together to cause demethylation of ribosomal DNA (rDNA) to promote rRNA transcription. Other than the Aurora kinase B gene, DHX33 deficiency led to alterations of 5-hmC in over 3,000 genes, including both positive and negative alterations. These data indicate a complicated role of DHX33 in epigenetics. Further

**FIG 7** Legend (Continued)
are shown in panel I. A representative result is shown from 3 separate experiments. (J) H1299 cells were infected by lentivirus encoding shSCR, shGadd45a, or shTet1. Five days postinfection, total RNA was extracted for RT-PCR analysis. (Top) Gadd45a and Aurora kinase B mRNA levels. (Bottom) Tet1 and Aurora kinase B mRNA levels. *, $P < 0.05$; $n = 3$. (K) Five days after infection by lentivirus, H1299 cells (shSCR, shRNA-DHX33) were subjected to ChIP analysis with S9.6 antibody, with IgG as a control. Samples were then analyzed by PCR and PAGE gel analysis. A representative result is shown from 3 separate experiments.

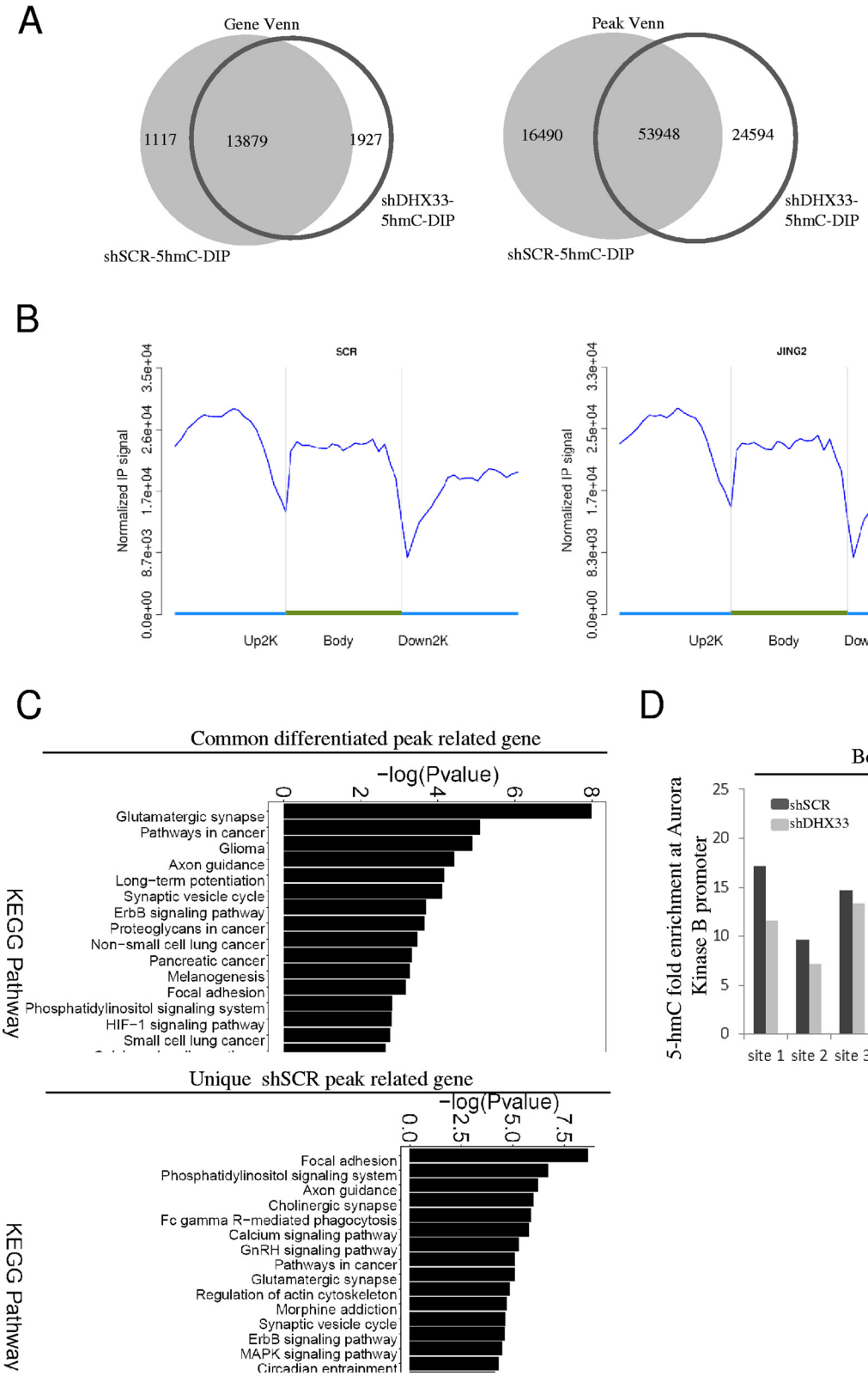


**FIG 8** DHX33 deficiency reduced the production of 5-hmC on specific genes. (A) H1299 cells were infected by lentivirus encoding either shSCR or shDHX33. Five days postinfection, cells were subjected to 5-hmC–DIP analysis. Differential 5-hmC levels correlating to the affected genes were compared between the control and DHX33 knockdown groups. Gene Venn values (left) and peak Venn values (right) are shown. (B) IP signals from 5-hmC-DIP on genes were compared according to 3 different gene domains (upper 2 kb, gene body, and downstream 2 kb) between the DHX33 knockdown (right) and the control group (left). *y*-axis data represent the fold enrichment of 5-hmC levels, with *x*-axis data showing different segments of genes. (C) (Top) KEGG pathway analysis for common differentiated peak-related genes. (Bottom) KEGG pathway analysis for the

(Continued on next page)

study is needed in order to address how DHX33 might negatively regulate gene expression.

Furthermore, with the SeqCap Epi enrichment system, we analyzed known 5-mC sites on genomes after DHX33 knockdown. Bisulfite treatment of DNA followed by DNA sequencing was incapable of differentiating 5-methylcytosine and 5-hydroxylmethylcytosine. We found that the total number of methylation/hydroxylation sites on cytosines increased significantly after DHX33 knockdown. For given gene loci, both increases and decreases of 5-mC/5-hmC levels were seen. Interestingly, DHX33 knockdown caused the percentages of two other methylcytosine forms (mCHG and mCHH) to increase dramatically, from 0.45% to 5.36% and 10.39%, respectively. Both forms of methylation are prevalent in plants but are rarely observed in mammals. The functional relevance remains to be revealed. Many of the affected genes belong to cancer-related pathways.

With the Aurora kinase B gene as an example, we discovered that DHX33, Gadd45a, and AP-2$\beta$ bound to the same proximal promoter region of Aurora kinase B. DHX33 is required to recruit Gadd45a and AP-2$\beta$ to its gene loci, which in turn recruit active RNA polymerase II for gene transcription. DHX33 deficiency reduced the levels of 5-hmC levels on the Aurora kinase B gene and thereby abolished its transcription.

To explain how Gadd45a can be recruited to Aurora kinase B gene promoters, we explored the relationship between DHX33 and R-loops. R-loops are RNA-DNA hybrid structures in which a coding or noncoding RNA hybridizes with one strand of DNA while displacing the other. Such structures are often found to be associated with open chromatin and are hyperaccessible. R-loops have previously been shown to be able to guide Gadd45a to specific gene loci for DNA demethylation. Genome profiling in cells found thousands of R-loop-dependent Tet1 binding sites at CpG islands (CGIs) (25). Gadd45a is therefore regarded as an epigenetic R-loop reader that recruits the demethylation machinery to promoter CGIs. In this study, we found that DHX33 is required to form the R-loop structure on gene promoters. DHX33 knockdown abolished the R-loop structure on the Aurora kinase B promoter. A genome-wide analysis of the R-loop present after DHX33 knockdown is needed to further elucidate the relationship between DHX33 and R-loops. On the basis of a previous publication, DHX33 does not appear to bind to R-loop structure directly in certain cell settings. It may not function to resolve aberrant R-loop structures in cells as other RNA helicases do (27).

Overall, our report reveals a novel mechanism explaining how DHX33 regulates gene expression at the genomic level. We present original evidence indicating that DHX33 alters epigenetic marks through a functional interaction with Gadd45a for specific gene loci. Further studies are needed to reveal in detail how DHX33 is able to couple its helicase activity to regulate epigenetics.

Our report also indicates the potential of DHX33 in cancer therapeutics. Importantly, DHX33 upregulates many genes to promote cell proliferation, migration, and survival and downregulates genes whose function(s) is to suppress cell growth/proliferation or to cause apoptosis. How this selectivity is conferred and how DHX33 could specifically regulate so many genes remain unknown. Given the pivotal role of DHX33 in cancer development, DHX33 should be further investigated as a potential molecular target in treating human cancers.

## MATERIALS AND METHODS

**Cell lines.** Human lung cancer cell lines H1299, H1975, and Calu-1 were purchased from ATCC and cultured in RPMI 1640 medium supplemented with 10% fetal bovine serum (FBS) and streptomycin-penicillin. The human embryonic kidney epithelial cell line HEK293T was purchased from ATCC and cultured in Dulbecco's modified Eagle's medium (DMEM [high glucose]) supplemented with 10% FBS and streptomycin-penicillin. All cells were maintained in a $CO_2$ (5%) incubator at 37°C with humidity.

**FIG 8** Legend (Continued)
unique shSCR peak-related genes. (D) The 5-hmC levels for Bcl-2 gene are shown in a bar graph. Multiple sites on the gene body were found to show downregulation of 5-hmC levels after DHX33 knockdown.

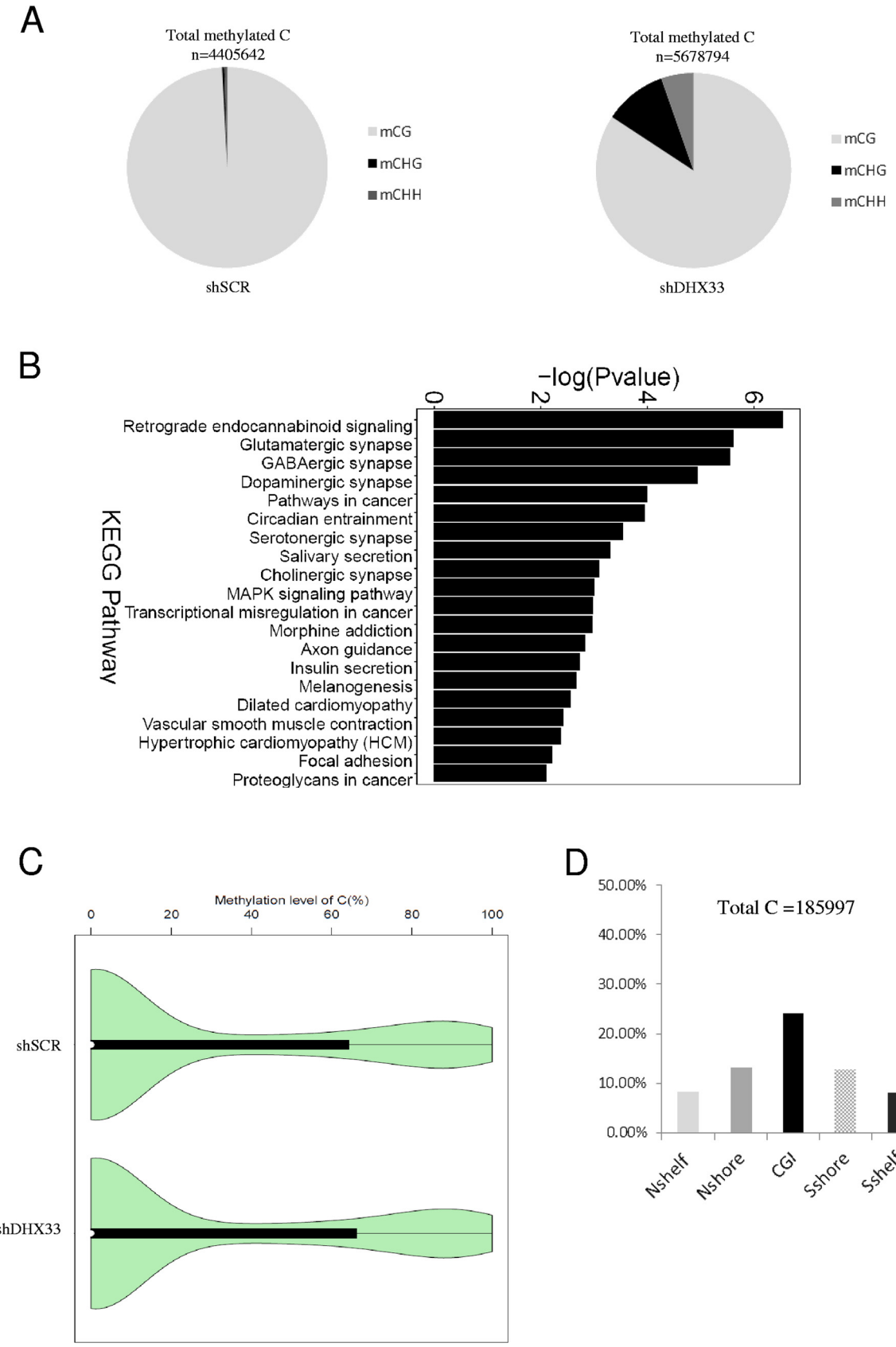


**FIG 9** DHX33 deficiency altered epigenetic marks on 5-C at the genomic level. (A) H1299 cells were infected by lentivirus encoding either shSCR or shDHX33. Five days postinfection, cells were subjected to targeted bisulfite sequencing. An SeqCap Epi enrichment system was used to evaluate

(Continued on next page)

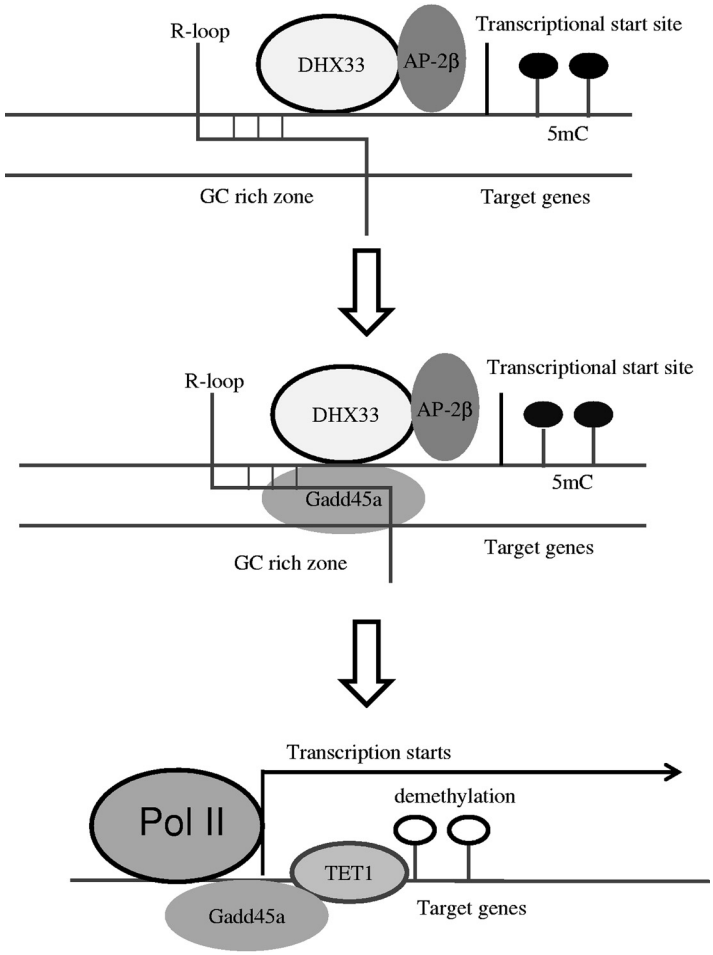


**FIG 10** Diagram showing how DHX33 causes DNA demethylation via Gadd45a. An R-loop in CGI functions to recruit Gadd45a in a DHX33-dependent manner. Transcription factor AP-2$\beta$ was also recruited to gene promoters. Gadd45a further recruits DNA demethylation enzymes such as Tet1. Tet1 is recruited to target gene sites, leading to DNA demethylation. Epigenetic alteration, together with AP-2$\beta$, eventually contributes to gene activation.

**Lentivirus production.** To produce lentivirus, pLKO.1-shRNA and virus packaging plasmids pCMV-VSV-G and pCMVΔR8.2 were transfected into HEK293T cells by the use of Lipofectamine 2000 reagent (Life Technologies). The shRNA sequences targeting human DHX33 were used as described previously (12). The shRNA sequences used to target human Tet1, Gadd45a, and Ing-1 were as follows (5′ to 3′): 1-shTet1, TTGTGCCTCTGGAGGTTATAA; 2-shTet1, GCAGCTAATGAAGGTCCAGAA; 1-shGadd45a, TTGCCGG GAAAGTCCCTACAT; and 2-shGadd45a, CCAGTGATTAATCTCCCTGAA. To produce lentivirus overexpressing DHX33, pLVX-FLAG-tagged wild-type DHX33 or K94R mutant DHX33 and packaging plasmids pCMV-VSV-G and pCMVΔR8.2 were cotransfected into HEK293T cells. At 48 h later, culture supernatant was collected and centrifuged at 2,000 rpm for 2 min. Virus was then aliquoted and frozen at −80°C.

**CRISPR/Cas9 plasmid construction.** An all-in-one vector encoding guide RNA and wild-type Cas9 protein, pSpCas9(BB)-2A-puro(PX459), was used for constructing guide RNA plasmids targeting the human DHX33 gene. The following DNA oligonucleotides were synthesized for cloning gRNA-DHX33 (all DNA oligonucleotides are presented 5′ to 3′): Exon1 F, CACCGCGATGAGGACCGCGTTGTCC; Exon1 R, AAACGGACAACGCGGTCCTCATCGC; Exon2 F, CACCGGAGATGGCAGCTACTCGACG; Exon2 R, AAACCGTC GAGTAGCTGCCATCTCC; Exon3 F, CACCGTTTTGGATGAAGCTCACGAA; Exon3 R, AAACTTCGTGAGCTTCAT CCAAAAC; Exon4 F, CACCGGGGTCGGCAGCATCCGATCC; and Exon4 R, AAACGGATCGGATGCTGCCGAC

**FIG 9** Legend (Continued)
the epigenetic marks in both shSCR and shDHX33 samples. The composition of methylated C in mCG, mCHG, and mCHH is shown with total methylation sites on the top. (B) KEGG pathway analysis for differentially methylated genes between the control and DHX33 knockdown groups. MAPK, mitogen-activated protein kinase. (C) Violin graph evaluating the methylation levels between the control and the DHX33 knockdown groups. (D) For differentially methylated sites (total, 185,997), results of analyses of their methylation sites are shown in the bar graph. Among them, CGI takes 24.34%.

CCC. Pairs of DNA oligonucleotides were annealed and then ligated into the BbsI restriction enzyme site. DNA sequencing was performed to ensure that the constructs were correct.

**Western blotting and immunoprecipitation.** For Western blotting, cells were lysed by the use of radioimmunoprecipitation assay (RIPA) buffer supplemented with protease and phosphatase inhibitors (Thermo Fisher). After incubation for 10 min on ice, cell lysates were further disrupted by sonication. Whole-cell extract was then subjected to SDS-PAGE using gel with a loading amount of 50 $\mu$g protein per sample. Proteins were then transferred onto a polyvinylidene difluoride membrane. Membranes were blocked in 5% nonfat milk diluted in 1× Tris-buffered saline with Tween 20 (TBST) buffer for 1 h at room temperature. Primary antibodies were diluted in 5% bovine serum albumin (BSA) (diluted in 1× TBST) and incubated with the membranes at 4°C overnight. Membranes were then rinsed with 1× TBST buffer multiple times and incubated with horseradish peroxidase (HRP)-labeled secondary antibodies mixed in 5% BSA (diluted in 1× TBST) at room temperature for 2 h. Blots were visualized with an ECL kit (Thermo Fisher).

For immunoprecipitation, cells were lysed by the use of EBC buffer (50 mM Tris-HCl [pH 8.0], 120 mM NaCl, 0.5% Nonidet P-40) supplemented with protease and phosphatase inhibitors (Thermo Fisher). After incubation for 10 min on ice, cell lysates were further disrupted by sonication. Whole-cell lysates were centrifuged at 13,000 rpm for 10 min at 4°C. Supernatants were adjusted to a concentration of approximately 1 mg/ml and incubated with 2 $\mu$g of the indicated antibody overnight at 4°C. Normal IgG was used as a control. The next day, protein A/G-conjugated beads were added and cell lysates were further incubated for 1 to 2 h at 4°C. Beads were then washed with EBC buffer 3 times followed by analysis.

The antibodies were sourced as follows: anti-DHX33 (A-3, for IP analysis) and anti-DHX33 (B-4, for immunofluorescence, immunohistochemistry, and Western blotting), Santa Cruz Biotechnology (sc-390574 and sc-390573); anti-DHX33 (for Western blotting), Bethyl (A300-800A); anti-pPOL II (phosphorylation on S2, for ChIP analysis), Abcam (ab-5095); anti-Gadd45a (sc-6850, for Western blotting and immunoprecipitation), Santa Cruz Biotechnology; anti-Gadd45a (ab180768, for immunofluorescence and Western blotting), Abcam; anti-S9.6 (MABE1095, for ChIP analysis), Merck Millipore; anti-Tet1 (GT1462, for ChIP and Western blotting), GeneTex; anti-Aurora kinase A (ab13824, for Western blotting and immunohistochemistry), Abcam; anti-Aurora kinase B (ab2254, for Western blotting and immunohistochemistry), Abcam; anti-GAPDH (anti-glyceraldehyde-3-phosphate dehydrogenase), Absin (abs830030); anti-FLAG (M2) antibody, Sigma (F1840); anti-Ki67 (ab15580, for immunohistochemistry), Abcam; anti-acetyl-histone H4, Merck Millipore (MABE1095).

**Quantitative real-time PCR.** The primers were all designed by the use of an online Realtime PCR Tool (IDT) and purchased from BGI (Shenzhen). Total RNA was extracted by the use of a High Pure RNA isolation kit (Roche) and then transcribed into cDNA using a PrimeScript mix kit (TaKaRa). Real-time PCR was performed with an ABI One Step Plus cycler that was managed with the corresponding software. To analyze mRNA levels, SYBR green Supermix (Bio-Rad) was used, and transcript quantification was calculated by determining the threshold cycle ($\Delta\Delta C_T$) value after normalization to the GAPDH values. Melting curve analysis was used to confirm the amplification of each product. The primer sequences for this study are shown as follows (5′ to 3′): GAPDH-FP, TGACAACGAATTTGGCTACA; GAPDH-RP, GTGGTC CAGGGGTCTTACTC; DHX33-FP, CGTCCTCCACAACCCTCCTT; DHX33-RP, AAAATTCTCTTTGCACCAATCCTT; Aurora kinase A-FP, GTACATGCTCCATCTTCCAGG; Aurora kinase A-RP, AAAGAACTCCAAGGCTCCAG; Aurora kinase B-FP, ACCCTTTGAGAGTGCATCAC; Aurora kinase B-RP, GAGCAGTTTGGAGATGAGGTC; GADD45a-FP, TGTAATCCTTGCATCAGTGT; GADD45a-RP, ATCTCCCTGAACGGTGAT; Tet1-FP, fTCTGTTGTT GTGCCTCTGGA; and Tet1-RP, GCCTTTAAAACTTTGGGCTTC.

**Immunofluorescence.** Cells were fixed with 10% formalin–10% methanol. Cells were then incubated with the first primary antibody at a 1:100 dilution. Secondary antibody conjugated with fluorescein isothiocyanate (FITC) was applied to facilitate the visualization of the first protein. After immunostaining with the first antibody was performed, the second primary antibody was further incubated at a dilution of 50. Secondary antibody conjugated with rhodamine was then applied to visualize the second protein. Cells were then counterstained with DAPI (4′,6-diamidino-2-phenylindole) before treatment with mounting media for visualization under a confocal microscope.

**Immunohistochemistry.** Mouse lung tissues were dissected and dehydrated, paraffin embedded, and further sliced based on standard protocols. Tissues were deparaffinized in xylene and rehydrated in a series of alcohol solutions with decreasing concentrations. The antigen was retrieved in Tris buffer (pH 9.0) in a steamer. Tissues were then incubated with 1% $H_2O_2$ in methanol to extinguish endogenous peroxidase. After blocking with 10% FBS was performed for 1 h at room temperature, tissues were incubated with primary antibody at 4°C overnight. Standard protocols were then followed with the use of a Dako kit according to the manufacturer's recommendation.

**Chromatin immunoprecipitation.** Cells were fixed with 1% formaldehyde at room temperature followed by addition of L-glycine to reach a final concentration of 0.125 M to stop formaldehyde cross-linking. Cell are then washed with 1× PBS and resuspended in cell lysis buffer (pH 8.1) containing 1% SDS, 10 mM EDTA, and 50 mM Tris, supplemented with protease and phosphatase inhibitor cocktails. Cell lysates were then subjected to extensive sonication to break chromatin. After centrifugation, cell lysates are diluted with EBC buffer at a 1:5 ratio. To preclear cell lysates, samples were incubated with sheared salmon sperm DNA and protein A/G beads. Immunoprecipitation was performed by incubation with 2 $\mu$g antibody at 4°C overnight in the presence of sheared salmon sperm DNA. Protein A/G beads were then added into the mixture, which was further incubated for 1 h. The beads were removed through centrifugation and were washed twice with RIPA buffer at 4°C and twice with RIPA buffer containing 500 mM NaCl at 4°C. For re-ChIP experiments, after the first immunoprecipitation and

washing, the beads were incubated with 75 $\mu$l of the first extraction buffer containing 10 mM Tris-HCl (pH 8.0), 2 mM EDTA, and 10 mM dithiothreitol (DTT) at 37°C for 30 min. After centrifugation, the eluent was then diluted 20-fold with cold EBC buffer for the second immunoprecipitation. After three washes with cold RIPA buffer, the beads were then extracted with a solution containing 1% SDS and 0.1 M $NaHCO_3$. The eluted solution was subjected to mixing, and 6 M NaCl was added to reach a final concentration of 0.3 M. To reverse cross-linking, samples were heated at 65°C for 5 h. After purification of DNA fragments by the use of a spin column (Qiagen QIAquick spin kit), DNA samples were analyzed by real-time quantitative PCR or by PCRs followed by agarose gel electrophoresis. The primer sequences used for ChIP in this study were as follows (5′ to 3′): AURKB_ChIP_FP, GCCCTTCCCTCCGTCCCTG; AURKB_ChIP_RP, CTGTCGTCAAACTTGGGACCCGTA; AURKA_ChIP_FP, GATTTTGTCCTCCGAGATCACC; AURKA_ChIP_RP, CC CAGCTGCAAGTTCTCCGTA; ART ChIP-FP, TCTTGGCCTTTACTCGCTGGAC; ART ChIP-RP, GCCCAGCGTCTTTT CTGCAT; BACH2 ChIP-FP, TCTGCTCTCCTTCCCCAGGTG; BACH2 ChIP-RP, CTTCCCGGCCACGAAAGACGA; DOCK3 ChIP-FP, CTGGCCCCAAACATTCACCACT; DOCK3 ChIP-RP, CGTGCCCCTCTCTCCTGGAT; IP6K1 ChIP-FP, CCAGCCACTCCGGGAACGAA; IP6K1 ChIP-RP, CCACTGGGTACGGATCAACAACA; RPS19 ChIP-FP, GCCA TCATAGTATTCTCCAC; RPS19 ChIP-RP, GTTTCCTTCTCCCGGAGTGT; SIRT6 ChIP-FP, ATTGCGCCACTGCACT CCA; SIRT6 ChIP-RP, GCTATCCATGTCCCCACAACCC; PGK1 ChIP-FP, GCTTTGTGCATTTCGTCCAGT; PGK1 ChIP-RP, CCAGCCTGAGCAACATAGCAA; PLK2 ChIP-FP, ACTCACTGGCCTACGCTCCTC; PLK2 ChIP-RP, ACA ACCGTGGGCCTTTGACA; RPL11 ChIP-FP, CAGGAGAATCGCTTGAACCC; and RPL11 ChIP-RP, fTTGAAAGCT CCCGAATCAGCA.

**ChIP-seq.** Fragmented DNA was constructed into a DNA library. Specifically, DNA fragments were first end repaired and adenylated at the 3′ ends and then ligated to adaptors. DNA was then enriched according to standard protocol and quantitated by the use of Qubit (Invitrogen). DNA was then diluted to a final concentration of 10 nM. DNA sequencing was performed with a Hiseq 2500 system (Illumina) after cBot cluster generation performed on the basis of the use of Hiseq 2500s of DNA samples.

**5-hmC-DIP.** DNA was extracted according to a standard protocol. After DNA quantitation by the use of Qubit (Invitrogen), approximately 2 $\mu$g of DNA was fragmented by the use of a Bioruptor. DNA fragments were then end repaired, adenylated at 3′ ends, and ligated to adaptors. About 1 $\mu$g of this DNA sample was subjected to immunoprecipitation with an equal amount of anti-5-hmC antibody (ab106918, Abcam) in SimpleDIP buffer based on a standard protocol. Equal amounts of ChIP-grade protein G magnetic beads were then added to precipitate the target DNA. After washing and elution were performed, the DNA was purified. After PCR amplification and enrichment, the DNA was quantitated by the use of Qubit, followed by cBot cluster generation and DNA sequencing performed with a Hiseq 2500 (Illumina) on the basis of the use of equal amounts of DNA samples.

**Targeted bisulfite sequencing for epigenetic analysis.** DNA was isolated and fragmented for DNA library construction as described previously. Equal amounts of DNA sample were then treated with bisulfite according to a standard protocol. A SeqCap Epi enrichment system was then used to capture target sites for enrichment. After PCR amplification, the samples were sequenced and evaluated on the basis of the epigenetic changes at target sites. Data were produced using an 83.9-Mb design.

**Bisulfite sequencing on AURKB gene promoter.** DNA was isolated from H1299 cells by the use of a DNA isolation kit (Tiangen Biotech, Beijing, China). DNA samples were treated for methylation analysis by the use of an EZ DNA methylation Gold kit according to the recommendation of the manufacturer (ZYMO Research, USA). To analyze the methylation sites on the Aurora kinase B gene promoters, the primers were designed for PCR amplification with the following sequences (5′ to 3′): FP, TTGTAATTTT AGTATTTTGGGAAGT, and BP, TTTTTAAAACAAATCTCTCTCTATC.

**Generation of DHX33 conditional knockout mice.** The DHX33 gene in the mouse genome spans a region about 20.5 kb on the reverse strand of chromosome 11. We used a CRISPR-Cas9 system to introduce two LoxP sites flanking exons 2 to 4 in order to conditionally knock out exons 2 to 4 in the DHX33 gene by the use of a Cre-loxP system. Introns 2 and 3 and introns 4 and 5 are big, and insertion of the lox element does not interfere with mRNA splicing. To minimize the possibility of disruption of DHX33 gene expression, both of the loxP sites were inserted into nonconserved regions. We used the following two guide RNA sequences for gene editing (5′ to 3′): forward sgRNA, CATGTATAATGGTAGG TAC, and reverse sgRNA, ATGTACCATGCATAGAGGCC. Both guide RNAs were cloned into pT7 plasmids and sequenced for confirmation. The targeting vector contains two loxP sites flanking exons 2 to 4 with a 5′ homologous arm and a 3′ homologous arm (each arm has ~1,400 bp). Zygote microinjection was performed following a standard protocol. Genotyping of founder mice was performed by PCR. For the 5′ LoxP site, the primers were as follows (5′ to 3′): FP, TGAATGGACATCTCGTCGTATCAGT, and RF, AATTCCACTTGCCGAAATTGAGTCT. The PCR product for the wild-type mice was 208 bp in size, while the PCR product for the mutant mice was 287 bp in size. For the 3′ LoxP site, the primers were as follows (5′ to 3′): FP, TGTGAGCTCTAGATTCAGTGAGAAC, and RP, TGTTTACCTCTAAATTGTCTCAGGA. The PCR product for the wild-type mice was 212 bp, while the PCR product for the mutant mice was 298 bp. The mutant allele was further confirmed by Southern blotting. The 5′ probe was amplified from a forward primer (5′-GTGCCTGTCTTTCTGTGTTGAATT-3′) and a reverse primer (5′-GAGACTAAAGTCATTTCGGATGC TG-3′). After StuI digestion, Southern blotting was performed with the labeled probe. For wild-type alleles, the size was 7.5 kb, while for the mutant allele; the size was 5.6 kb. The 3′ probe was amplified by the use of a forward primer (5′-TAAATAGATTCAACAGTTGCTG-3′) and a reverse primer (5′-TGGGTTCAGCTCATTTTTGAAAGG-3′). After NcoI digestion, Southern blotting was performed with the labeled probe. For the wild-type allele, the size was 6.1 kb, while for the mutant allele, the size was 5.1 kb.

**Adenovirus infection.** All mouse maintenance, breeding, and experimental procedures followed the Jackson Laboratory standard guidelines. Adenovirus was purchased from Vigene (Shandong, China). Both adeno-LacZ and adeno-Cre have titers of $1.0 \times 10^{11}$ PFU/ml. To set up a lung cancer model for use with

K-Ras (G12D-LSL) mice, we followed a protocol that was described previously (28). Briefly, approximately $1 \times 10^7$ PFU adenovirus encoding Cre recombinase was mixed with minimal essential medium (MEM) and $CaCl_2$ for precipitation. After mice were anesthetized by treatment with avertin through intraperitoneal injection, viruses were directly administered through nasal inhalation into mouse lungs. At 8 weeks after virus delivery, mice in each group were sacrificed and subjected to lung dissection for analysis.

**Statistical analysis.** Data are presented as means ± standard deviations (SD). Statistical significance was determined using Student's *t* test, with a *P* value of $<0.05$ considered significant.

**Data availability.** We certify that we comply with ASM's data policy. Data will be made publicly available upon publication and upon request for peer review.

## SUPPLEMENTAL MATERIAL

Supplemental material is available online only.

**SUPPLEMENTAL FILE 1**, XLS file, 0.5 MB.

**SUPPLEMENTAL FILE 2**, XLS file, 1.5 MB.

**SUPPLEMENTAL FILE 3**, XLSX file, 0.1 MB.

**SUPPLEMENTAL FILE 4**, XLSX file, 0.03 MB.

**SUPPLEMENTAL FILE 5**, XLS file, 5.2 MB.

**SUPPLEMENTAL FILE 6**, XLS file, 4.6 MB.

**SUPPLEMENTAL FILE 7**, XLS file, 0.2 MB.

## ACKNOWLEDGMENTS

We thank the support and the core facility in SUSTech and the Shenzhen Rozman International Institute of Translational Medicine.

This work was supported by the Science and Technology Innovation Committee of Shenzhen Municipality (grant no. JCYJ20170307110713487 and CKCY2017072116462727 to Y.Z.) and Guangdong Provincial Science and Technology Department (grant no. 2017A020211024 to Y.Z.). The funder (KeYe Life Technologies) provided support in the form of reagents purchasing, RNA sequencing, and ChIP-seq, as well as the publication fee.

We declare that we have no competing financial interests.

## REFERENCES

1. Fuller-Pace FV. 1994. RNA helicases: modulators of RNA structure. Trends Cell Biol 4:271–274. https://doi.org/10.1016/0962-8924(94)90210-0.
2. Cai W, Xiong Chen Z, Rane G, Satendra Singh S, Choo Z, Wang C, Yuan Y, Zea Tan T, Arfuso F, Yap CT, Pongor LS, Yang H, Lee MB, Cher Goh B, Sethi G, Benoukraf T, Tergaonkar V, Prem Kumar A. 2017. Wanted DEAD/H or alive: helicases winding up in cancers. J Natl Cancer Inst 109:djw278. https://doi.org/10.1093/jnci/djw278.
3. Fuller-Pace FV. 2013. DEAD box RNA helicase functions in cancer. RNA Biol 10:121–132. https://doi.org/10.4161/rna.23312.
4. Wang X, Ge W, Zhang Y. 2019. Recombinant DHX33 protein possesses dual DNA/RNA helicase activity. Biochemistry 58:250–258. https://doi.org/10.1021/acs.biochem.8b00166.
5. Mitoma H, Hanabuchi S, Kim T, Bao M, Zhang Z, Sugimoto N, Liu YJ. 2013. The DHX33 RNA helicase senses cytosolic RNA and activates the NLRP3 inflammasome. Immunity 39:123–135. https://doi.org/10.1016/j.immuni.2013.07.001.
6. Zhang Y, Forys JT, Miceli AP, Gwinn AS, Weber JD. 2011. Identification of DHX33 as a mediator of rRNA synthesis and cell growth. Mol Cell Biol 31:4676–4691. https://doi.org/10.1128/MCB.05832-11.
7. Zhang Y, You J, Wang X, Weber J. 2015. The DHX33 RNA helicase promotes mRNA translation initiation. Mol Cell Biol 35:2918–2931. https://doi.org/10.1128/MCB.00315-15.
8. Fu J, Liu Y, Wang X, Yuan B, Zhang Y. 2017. Role of DHX33 in c-Myc-induced cancers. Carcinogenesis 38:649–660. https://doi.org/10.1093/carcin/bgx041.
9. Wang J, Feng W, Yuan Z, Weber JD, Zhang Y. 12 August 2019, posting date. DHX33 interacts with AP-2beta to regulate Bcl-2 gene expression and promote cancer cell survival. Mol Cell Biol https://doi.org/10.1128/MCB.00017-19.
10. Yuan B, Wang X, Fan C, You J, Liu Y, Weber JD, Zhong H, Zhang Y. 2016. DHX33 transcriptionally controls genes involved in the cell cycle. Mol Cell Biol 36:2903–2917. https://doi.org/10.1128/MCB.00314-16.
11. Tian QH, Zhang MF, Luo RG, Fu J, He C, Hu G, Zeng JS. 2016. DHX33 expression is increased in hepatocellular carcinoma and indicates poor prognosis. Biochem Biophys Res Commun 473:1163–1169. https://doi.org/10.1016/j.bbrc.2016.04.033.
12. Wang H, Yu J, Wang X, Zhang Y. 2019. The RNA helicase DHX33 is required for cancer cell proliferation in human glioblastoma and confers resistance to PI3K/mTOR inhibition. Cell Signal 54:170–178. https://doi.org/10.1016/j.cellsig.2018.12.005.
13. Chen ZX, Riggs AD. 2011. DNA methylation and demethylation in mammals. J Biol Chem 286:18347–18353. https://doi.org/10.1074/jbc.R110.205286.
14. Lyko F. 2018. The DNA methyltransferase family: a versatile toolkit for epigenetic regulation. Nat Rev Genet 19:81–92. https://doi.org/10.1038/nrg.2017.80.
15. Deaton AM, Bird A. 2011. CpG islands and the regulation of transcription. Genes Dev 25:1010–1022. https://doi.org/10.1101/gad.2037511.
16. Ito S, Shen L, Dai Q, Wu SC, Collins LB, Swenberg JA, He C, Zhang Y. 2011. Tet proteins can convert 5-methylcytosine to 5-formylcytosine and 5-carboxylcytosine. Science 333:1300–1303. https://doi.org/10.1126/science.1210597.
17. Guo JU, Su Y, Zhong C, Ming GL, Song H. 2011. Emerging roles of TET proteins and 5-hydroxymethylcytosines in active DNA demethylation and beyond. Cell Cycle 10:2662–2668. https://doi.org/10.4161/cc.10.16.17093.
18. Tan L, Shi YG. 2012. Tet family proteins and 5-hydroxymethylcytosine in development and disease. Development 139:1895–1902. https://doi.org/10.1242/dev.070771.
19. Tahiliani M, Koh KP, Shen Y, Pastor WA, Bandukwala H, Brudno Y, Agarwal S, Iyer LM, Liu DR, Aravind L, Rao A. 2009. Conversion of 5-methylcytosine to 5-hydroxymethylcytosine in mammalian DNA by MLL partner TET1. Science 324:930–935. https://doi.org/10.1126/science.1170116.

20. Barreto G, Schäfer A, Marhold J, Stach D, Swaminathan SK, Handa V, Döderlein G, Maltry N, Wu W, Lyko F, Niehrs C. 2007. Gadd45a promotes epigenetic gene activation by repair-mediated DNA demethylation. Nature 445:671–675. https://doi.org/10.1038/nature05515.
21. Niehrs C, Schafer A. 2012. Active DNA demethylation by Gadd45 and DNA repair. Trends Cell Biol 22:220–227. https://doi.org/10.1016/j.tcb.2012.01.002.
22. Kienhofer S, Musheev MU, Stapf U, Helm M, Schomacher L, Niehrs C, Schafer A. 2015. GADD45a physically and functionally interacts with TET1. Differentiation 90:59–68. https://doi.org/10.1016/j.diff.2015.10.003.
23. Schafer A, Karaulanov E, Stapf U, Doderlein G, Niehrs C. 2013. Ing1 functions in DNA demethylation by directing Gadd45a to H3K4me3. Genes Dev 27:261–273. https://doi.org/10.1101/gad.186916.112.
24. Sytnikova YA, Kubarenko AV, Schafer A, Weber AN, Niehrs C. 2011. Gadd45a is an RNA binding protein and is localized in nuclear speckles. PLoS One 6:e14500. https://doi.org/10.1371/journal.pone.0014500.
25. Arab K, Karaulanov E, Musheev M, Trnka P, Schafer A, Grummt I, Niehrs C. 2019. GADD45A binds R-loops and recruits TET1 to CpG island promoters. Nat Genet 51:217–223. https://doi.org/10.1038/s41588-018-0306-6.
26. Zhong J, Li X, Cai W, Wang Y, Dong S, Yang J, Zhang J, Wu N, Li Y, Mao F, Zeng C, Wu J, Xu X, Sun ZS. 2017. TET1 modulates H4K16 acetylation by controlling auto-acetylation of hMOF to affect gene regulation and DNA repair function. Nucleic Acids Res 45:672–684. https://doi.org/10.1093/nar/gkw919.
27. Cristini A, Groh M, Kristiansen MS, Gromak N. 2018. RNA/DNA hybrid interactome identifies DXH9 as a molecular player in transcriptional termination and R-loop-associated DNA damage. Cell Rep 23:1891–1905. https://doi.org/10.1016/j.celrep.2018.04.025.
28. DuPage M, Dooley AL, Jacks T. 2009. Conditional mouse lung cancer models using adenoviral or lentiviral delivery of Cre recombinase. Nat Protoc 4:1064–1072. https://doi.org/10.1038/nprot.2009.95.